ELSEVIER

Contents lists available at ScienceDirect

Biomaterials

journal homepage: www.elsevier.com/locate/biomaterials



Amino acid-based compound activates atypical PKC and leptin receptor pathways to improve glycemia and anxiety like behavior in diabetic mice



Aejin Lee^{a,1}, Yuan Sun^{b,1}, Tao Lin^b, No-Joon Song^a, McKensie L. Mason^b, Jacob H. Leung^a, Devan Kowdley^a, Jennifer Wall^a, Alessandro Brunetti^b, Julie Fitzgerald^c, Lisa A. Baer^d, Kristin I. Stanford^d, Joana Ortega-Anaya^e, Laisa Gomes-Dias^f, Bradley Needleman^g, Sabrena Noria^g, Zachary Weil^c, Joshua J. Blakeslee^f, Rafael Jiménez-Flores^e, Jon R. Parquette^{b,2}, Ouliana Ziouzenkova^{a,2,*}

- ^a Department of Human Sciences, The Ohio State University, Columbus, OH, 43210, USA
- ^b Department of Chemistry and Biochemistry, The Ohio State University, Columbus, OH, 43210, USA
- ^c Department of Neuroscience, Wexner Medical Center, The Ohio State University, Columbus, OH, 43210, USA
- d Department of Physiology and Cell Biology, Dorothy M. Davis Heart and Lung Research Institute, The Ohio State University, Columbus, OH, 43210, USA
- ^e Department of Food Science and Technology, The Ohio State University, Columbus, OH, 43210, USA
- Department of Horticulture and Crop Science, Ohio Agricultural Research and Development Center (OARDC), The Ohio State University, Columbus, OH, 44691, USA
- ⁸ The Comprehensive Weight Management and Bariatric Surgery Program, Center for Minimally Invasive Surgery, The Ohio State University Wexner Medical Center, Columbus, OH, 43210, USA

ARTICLE INFO

Keywords: Nanofibers Amino acids Diabetes Hyperglycemia Leptin receptors PKC

ABSTRACT

Differences in glucose uptake in peripheral and neural tissues account for the reduced efficacy of insulin in nervous tissues. Herein, we report the design of short peptides, referred as amino acid compounds (AAC) with and without a modified side chain moiety. At nanomolar concentrations, a candidate therapeutic molecule, AAC2, containing a 7-(diethylamino) coumarin-3-carboxamide side-chain improved glucose control in human peripheral adipocytes and the endothelial brain barrier cells by activation of insulin-insensitive glucose transporter 1 (GLUT1). AAC2 interacted specifically with the leptin receptor (LepR) and activated atypical protein kinase C zeta (PKCc) to increase glucose uptake. The effects induced by AAC2 were absent in leptin receptor-deficient predipocytes and in *Lepr^{db}* mice. In contrast, AAC2 established glycemic control altering food intake in leptin-deficient *Lep^{ob}* mice. Therefore, AAC2 activated the LepR and acted in a cytokine-like manner distinct from leptin. In a monogenic *Ins2*^{Akita} mouse model for the phenotypes associated with type 1 diabetes, AAC2 rescued systemic glucose uptake in these mice without an increase in insulin levels and adiposity, as seen in insulin-treated *Ins2*^{Akita} mice. In contrast to insulin, AAC2 treatment increased brain mass and reduced anxiety-related behavior in *Ins2*^{Akita} mice. Our data suggests that the unique mechanism of action for AAC2, activating LepR/PKCc/GLUT1 axis, offers an effective strategy to broaden glycemic control for the prevention of diabetic complications of the nervous system and, possibly, other insulin insensitive or resistant tissues.

1. Introduction

Glucose is a critical substrate of both anabolic synthetic processes and catabolic energy utilization pathways. Glucose uptake is regulated by variety of molecules ranging from plant metabolites [1,2], lipids [3], amino acids and their derivatives [4], di- and poly-peptides [5,6], cytokines [7], growth factors [8], and hormones [9–12]. Nonetheless,

neuroendocrine pathways play a chief role in the adaptation of glucose uptake to cellular requirements. In peripheral tissues, insulin regulates the major glucose transporter (GLUT) 4, supplying up to 70% and 10% of post prandial glucose to muscle and adipose tissues, respectively [13]. Insulin is a growth hormone that streamlines glucose utilization for anabolic processes, including growth and energy storage in fat [13,14]. Dysfunctional components of the insulin signaling pathway,

^{*} Corresponding author. 1787 Neil Avenue, 331A Campbell Hall, Columbus, OH, 43210, USA.

E-mail address: ziouzenkova.1@osu.edu (O. Ziouzenkova).

¹ Both authors contributed equally to this work.

² Both laboratories contributed equally to this work.

including deficient insulin production, misfolding of insulin 2 in Ins2^{Aktia} mice, disruption of the insulin receptor response, and deficiency in GLUT4 in some tissues, lead to diabetes in humans and other animals [13,15]. In type 1 diabetes (T1D), insulin has been a principal therapy for 100 years that effectively controls peripheral glucose homeostasis to support growth in children as well as lipogenesis and other anabolic processes in all age groups [13,14]. Alternatively to insulin, leptin can also regulate GLUT4 [16], although this pathway utilizes glucose for catabolic processes [17]. Crosstalk between insulin and leptin establishes glucose homeostasis under physiological conditions [18,19]. In T1D leptin production is often reduced [20]. Leptin treatment could compensate for peripheral GLUT4-dependent glucose uptake in insulindeficient mouse models of T1D [21,22] and under insulin resistant conditions in Lep^{ob} and lipodystrophic mice [23] and patients [24]; however, leptin resistant-states in obese patients and under inflammatory conditions limit applications of leptin for treatment of type 2 diabetes (T2D).

Neural tissue is another major glucose-consuming tissue (up to 20% of daily glucose), relying on glucose as the primary energy source [25]. The regulation of glucose uptake is principally different in neural vs. peripheral tissues [26]. Insulin-insensitive transporters GLUT1 and GLUT3 are abundantly expressed in the brain and brain vasculature [27,28]. Specifically, vascular endothelial cells and astrocytes comprising the blood brain barrier depend on GLUT1 [28]. GLUT1 is the principal transporter for glucose in neural tissues and a deficiency in GLUT1 in mice [29] and in humans [30] leads to irreversible neuronal damage [30]. Leptin also regulates the expression and translocation of GLUT1 in T cells [31], although the relevance of this pathway in the central nervous system (CNS) is unknown. Diabetes deactivates GLUT1 by several mechanisms including the reduction of leptin levels [20], loss of GLUT1-regulating amino acids [32], and/or the oxidative modification of a phosphorylation site on protein kinase C (PKC), which is responsible for the GLUT1 translocation [33]. Optimized neural function requires the concerted action of GLUT1 with GLUT4 and many other glucose and sodium-dependent transporters supplying glucose to specific regions of the brain [25,26,34]. Given that glucose uptake in neurons is not chiefly dependent on insulin, ablation of the insulin receptor (InsR) pathway in neurons does not abolish their function and spatial learning and memory remain intact in mice [35]. Moreover, in diabetes, chronic hyperinsulinemia can desensitize GLUT4 translocation and decrease glucose uptake via this mechanism [36]. Insulin stimulation leads to reciprocal uptake of glucose in peripheral tissues compared to brain [37] that contributes to hypoglycemic episodes and energy deprivation states in neurons [14].

Several devices, therapeutics and, materials have been developed to improve insulin release, secretion, efficacy, or stability that improve canonic GLUT4-mediated glucose uptake [14,38]. However, diminished regulation of glucose by GLUT1 in peripheral and neural tissue in diabetic states could be an additional factor for suboptimal insulin efficacy in these tissues. Currently, drug regimens optimize systemic glucose control and cannot prevent debilitating neurodegeneration that contributes to the development of retinopathies, neuropathies [39], and CNS damage [40] in patients with diabetes. Cognitive deficits occur across all age groups with T1D and T2D [41]. In children, they manifest rapidly, typically within 2 years of a diagnosis of T1D [42]. Adults with diabetes initially develop early cognitive decrements and mild cognitive impairments [41]; that progress to dementia in 80% of patients with impaired cerebral glucose metabolism [43]. A meta-analysis of studies with over 2 million participants indicates a 1.73 fold greater risk for the development of all types of dementia in patients with diabetes compared to those without this disease [41]. The goal of our study was to identify compounds regulating alternative pathways for glucose uptake that can work in conjunction with current insulin therapies. Natural amino acids and di- and poly-peptides could have glycemic properties [4-6]. Some polypeptides, isolated from natural sources such as M. Charantia, and amino acids display "insulinomimetic" properties that lead to decreased serum glucose levels [44]. In particular, lysine ingested at very high physiological doses with glucose, significantly attenuates the glucose response without a concomitant increase in insulin levels [45]. However, their proteolytic degradation could limit the efficacy of dietary peptides. Similarly, plant derivatives [46], particularly coumarins, have been shown to have antidiabetic activity, albeit at very high dosage levels [1,47]. The therapeutic effect of natural coumarins and their derivatives have been reported to emerge from repair of pancreatic β -cell damage, improved insulin signaling, and/or anti-oxidative/anti-inflammatory protection [47,48]. The glycemic and inflammatory properties of molecules comprised of both amino acids and coumarin have not been investigated.

Here, we report a strategy to develop new materials based on amino acid compounds (AAC) with modified side chains that can self-assemble into nanostructures to enhance glucose uptake in insulin-insensitive and insulin resistant states. We demonstrate the efficacy of a prototype (AAC2) peptide, which rescues mice with the hyperglycemia phenotypes associated with T1D and T2D leading and leads to improved neurological outcomes.

2. Materials and methods

2.1. Materials

2.1.1. Synthesis of AAC

2.1.1.1. Reagents. 4-Diethylaminosalicylaldehyde, diethylmalonate diisopropylethylamine (DIPEA) and trifluoroacid (TFA) were purchased from Oakwood Chemical. Benzyl alcohol was bought from Mallinckrodt. Succinic anhydride, 4-dimethylaminopyridine (DMAP), 1,3-diisopropylcarbodiimide (DIC), 1- hydroxybenzotriazole (HOBt), triethylsiliane (TES), 2-(1H-benzotriazol-1-yl)-1,1,3,3-tetramethyluronium hexafluorophosphate (HBTU) and amino acids were purchased from Chem Impex Int'l Inc. Rink amide resin was purchased from ChemPep. Benzoic acid and all solvents were purchased from Fisher Scientific. The synthesis of starting materials and peptides, including 7-(diethylamino)-3-coumarin carboxylic acid (DAC) [49] and benzyl succinic acid [50] are outlined (Fig. S1) and described in the Supplementary Materials.

2.1.1.2. Synthesis. The syntheses of AAC1-7 are outlined (Fig. S1). First, the peptide is synthesized using a solid phase peptide coupling protocol on Rink amide resin (0.8 g/mmol). All amino acids were coupled using Fmoc-protected amino acids, DIC and HOBt, which were combined in DMF and reacted for 2 h. The Fmoc group was removed using 20% piperidine in DMF and the Mtt group was deprotected using TFA/TES/DCM (2:1:97). Boc, tBu and Pbf groups were removed using TFA/TES/H₂O (94:5:1) at the final cleaving step. Benzyl succinic acid, DAC and benzoic acid were coupled on the deprotected lysine side chain using HOBt, HBTU and DIPEA to yield AAC1-7 respectively. The final peptides were cleaved with TFA/TES/H₂O (94:5:1). After cleavage from the solid support, all AAC peptides were purified by high performance liquid chromatography (HPLC; Ultimate 3000 Thermo Fisher Scientific Waltham, MA) using Hypersil Gold C8 reverse-phase column (Thermo Fisher Scientific). AAC structures were validated using ¹H NMR at 700 MHz and ¹³C NMR at 176 MHz on a Bruker Advance III HD Ascend 700 MHz instrument and mass spectroscopy (Bruker MicrOTOF mass spectrometer) (Fig. S1).

AAC1 ¹H NMR (700 MHz, DMSO- d_6) δ 7.90 (2H, d, J = 7.5 Hz), 7.82 (1H, t, J = 5.5 Hz), 7.80 (1H, d, J = 8.0 Hz), 7.73 (1H, d, J = 7.5 Hz), 7.71(1H, d, J = 7.5 Hz), 7.64 (2H, bs), 7.51(1H, d, J = 8.1 Hz), 7.42(2H, t, J = 7.4 Hz), 7.28–7.39 (8H, m), 7.02 (1H,s), 5.07 (2H,s), 4.29 (2H, m), 4.23 (1H, t, J = 7.07 Hz), 4.18 (1H, m), 4.00 (1H, m), 2.99 (2H, m), 2.76 (2H, m), 2.55 (2H, t, J = 6.9 Hz), 2.36 (2H, t, J = 6.9 Hz), 1.64 (2H, m), 1.52 (4H, m), 1.21–1.39 (6H, m); ¹³C NMR (176 MHz, DMSO- d_6) δ 173.98, 172.73, 172.04, 170.85, 156.45, 144.37, 144.19, 141.20, 136.70, 128.86, 128,40, 128.26, 128.12,

127.56, 127.54, 125.76, 125.71, 120.61, 120.60, 66.08, 65.83, 54.89, 52.58, 47.14, 39.19, 38.92, 32.31, 31.71, 30.27, 29.52, 29.31, 27.03, 23.11, 22.80; ESI-MS for $C_{38}H_{47}N_5O_7 \left[M+H\right]^+$ calculated 686.3548; found 686.3567.

AAC2 ¹H NMR (700 MHz, DMSO- d_6) δ 8.63 (1H, s), 7.87 (2H, d, J=7.5 Hz), 7.85 (1H, d, J=8.0 Hz), 7.77 (3H, bs), 7.73 (1H, d, J=7.5 Hz), 7.70 (1H, d, J=7.4 Hz), 7.65 (1H, d, J=9.0 Hz), 7.52 (1H, d, J=8.1 Hz), 7.41 (2H, t, J=7.2 Hz), 7.33 (2H, t, J=7.4 Hz), 7.04 (s, 1H), 6.79 (1H, dd, J=9.0, 2.2 Hz), 6.58 (1H, d, J=2.0 Hz), 4.29 (2H, m), 4.21 (2H, m), 4.01 (1H, m), 3.46 (4H, m), 3.27 (2H, m), 2.77 (2H, m), 1.67 (2H, m), 1.48–1.59 (6H, m), 1.33 (4H, m),1.13 (6H, t, J=7.0 Hz); ¹³C NMR (176 MHz, DMSO- d_6) δ 174.03, 172.08, 162.56, 162.25, 157.65, 156.45, 152.84, 144.39, 144.18, 141.18, 131.98, 127.54, 127.52, 125.76, 125.70, 120.55, 110.56, 109.90, 108.11, 96.28, 66.07, 54.94, 52.56, 47.14, 44.78, 39.28, 39.15, 32.31, 31.70, 29.35, 27.02, 23.20, 22.80, 12.74; ESI-MS for $C_{41}H_{50}N_6O_7$ [M +H] $^+$ calculated 739.3814; found 739.3818.

AAC3 ¹H NMR (700 MHz, DMSO- d_6) δ 8.48 (1H, t, J = 5.5 Hz), 8.01 (1H, d, J = 8.1 Hz), 7.99 (1H, d, J = 8.1 Hz), 7.94 (1H, d, J = 8.0 Hz), 7.91 (2H, d, J = 7.6 Hz), 7.84 (2H, d, J = 7.14 Hz), 7.72 (1H, d, J = 7.3 Hz), 7.71(1H, d, J = 7.0 Hz), 7.68 (2H, bs), 7.63 (2H, bs)bs), 7.51 (1H, t, J = 7.4 Hz), 7.50 (1H, d, J = 8.1 Hz), 7.44 (2H, t, J = 7.9 Hz), 7.42 (2H, t, J = 7.5 Hz), 7.33 (2H, t, J = 7.5 Hz), 7.20-7.25 (5H, m), 7.18 (1H, t, J = 6.8 Hz), 7.05 (1H, s), 4.54 (1H, m), 4.30 (1H, m), 4.23 (3H, m), 4.16 (1H, m), 3.98 (1H, m), 3.25 (2H, m), 3.05 (1H, m), 2.68-2.83 (5H, m), 1.70 (1H, m), 1.44-1.63 (12H, m), 1.23–1.33 (6H, m); 13 C NMR (176 MHz, DMSO- d_6) δ 173.85, 172.30, 171.80, 171.09, 166.65, 156.48, 144.29, 144.26, 141.20, 138.05, 135.09, 131.51, 129.63, 128.70, 128.50, 128.14, 127.60, 127.54, 126.72, 125.77, 125.73, 120.65, 120.61, 66.06, 54.78, 54.22, 52.89, 52.65, 47.12, 39.19, 37.80, 32.38, 31.98, 31.71, 29.40, 27.10, 23.27, 22.98, 22.55; ESI-MS for $C_{49}H_{62}N_8O_7$ [M+H]⁺ calculated 875.4814; found 875.4814.

AAC4 1 H NMR (700 MHz, DMSO- 4 6) δ 8.64 (1H, s), 8.62(1H, t, J=5.7 Hz), 7.88 (2H, d, J=7.5 Hz), 7.83 (1H, d, J=8.0 Hz), 7.73 (1H, d, J=7.5 Hz), 7.71 (1H, d, J=7.5 Hz), 7.67 (1H, d, J=9.0 Hz), 7.57 (1H, d, J=8.1 Hz), 7.41 (2H, t, J=7.4 Hz), 7.37 (1H, s), 7.33 (2H, d, J=7.4 Hz), 7.02 (1H, s), 6.79 (1H, dd, J=9.0, 2.2 Hz), 6.60 (1H, d, J=2.1 Hz), 4.26 (2H, m), 4.19 (2H, m), 4.02 (1H, m), 3.46 (5H, m), 3.26 (2H, m), 2.27 (2H, t, J=7.9 Hz), 1.92 (1H, m), 1.76 (1H, m), 1.68 (1H, m), 1.56 (1H, m), 1.50 (2H, m), 1.31 (2H, m), 1.14 (6H, t, J=7.0 Hz); 13 C NMR (176 MHz, DMSO- 4 6) δ 174.43, 173.90, 171.65, 162.53, 162.24, 157.65, 156.39, 152.84, 148.10, 144.38, 144.20, 141.16, 132.00, 128.09, 127.55, 125.79, 125.76, 120.55, 110.57, 109.95, 108.13, 96.32, 66.15, 54.44, 52.58, 47.11, 44.78, 39.25, 32.25, 30.70, 29.35, 27.75, 23.18, 12.78; ESI-MS for $C_{40}H_{45}N_{5}O_{9}$ [M+23] $^{+}$ calculated 762.3109; found 762.3107.

AAC5 1 H NMR (700 MHz, DMSO- d_{6}) δ 8.64 (1H, s), 7.89 (2H, t, J=7.6 Hz), 7.83 (1H, d, J=8.0 Hz), 7.73 (1H, d, J=7.5 Hz), 7.70 (1H, d, J=7.5 Hz), 7.67 (1H, d, J=9.1 Hz), 7.57 (1H, d, J=8.2 Hz), 7.52 (1H, t, J=5.5 Hz), 7.41 (2H, t, J=7.4 Hz), 7.32 (2H, t, J=7.4 Hz), 7.04 (1H, s), 6.80 (1H, dd, J=9.0, 2.3 Hz), 6.59 (1H, d, J=2.2 Hz), 4.29 (2H, m), 4.22 (2H, m), 4.04 (1H, m), 3.48 (4H, m), 3.37 (2H, m), 3.10 (2H, m), 1.67–1.72 (2H, m), 1.44–1.60 (6H, m), 1.26–1.35 (2H, m), 1.14 (6H, t, J=7.1 Hz); 13 C NMR (176 MHz, DMSO- d_{6}) δ 173.90, 171.80, 162.56, 157.66, 157.13, 156.40, 152.87, 144.38, 144.15, 141.18, 132.01, 128.10, 127.55, 125.70, 120.57, 110.60, 109.98, 108.12, 96.30, 66.12, 54.76, 52.54, 47.13, 44.79, 40.91, 39.29, 32.35, 29.54, 29.36, 25.56, 23.13, 12.77; C_{41} H₅₀N₈O₇ [M +H] $^{+}$ calculated 767.3875; found 767.3865.

AAC6 ¹H NMR (700 MHz, DMSO- d_6) δ 7.91 (2H, d, J = 7.4 Hz), 7.72 (2H, d, J = 6.4 Hz), 7.50 (1H, d, J = 8.0 Hz), 7.43 (2H,t, J = 7.5 Hz), 7.38 (1H, s), 7.34 (2H, t, J = 7.4 Hz), 7.04 (1H,s), 4.14–4.32 (4H, m), 4.00 (1H, m), 2.75 (4H, m), 1.65 (2H, m), 1.49–1.59 (6H, m), 1.31 (4H, m); ¹³C NMR (176 MHz, DMSO- d_6) δ 173.81, 172.19, 156.47, 144.31, 144.25, 141.20, 128.14, 127.55, 125.77,

125.75, 120.64, 120.61, 66.07, 54.87, 52.42, 47.13, 39.17, 32.02, 31.67, 27.12, 27.06, 22.89, 22.65; ESI-MS for $C_{27}H_{37}N_5O_4$ [M+H] $^+$ calculated 496.2918; found 496.2922.

AAC7 1 H NMR (700 MHz, DMSO- d_{6}) δ 8.42 (1H, t, J=5.9 Hz), 7.90 (2H, d, J=7.1 Hz), 7.82 (2H, d, J=7.4 Hz), 7.73 (1H, d, J=7.4 Hz), 7.71 (1H, d, J=7.6 Hz), 7.52 (2H, d, J=7.8 Hz), 7.50 (1H, d, J=7.3 Hz), 7.40–7.46 (5H, m), 7.38 (1H, s), 7.33 (2H, t, J=7.4 Hz), 7.03 (1H, s), 4.28 (2H, m), 4.22 (2H, m), 4.00 (1H, m), 3.23 (2H, m), 2.76 (2H, m), 1.62–1.72 (2H, m), 1.47–1.59 (7H, m), 1.27–1.37 (5H,m); 13 C NMR (176 MHz, DMSO- d_{6}) δ 173.98, 172.04, 166.55, 156.45, 144.38, 144.20, 141.20, 135.15, 131.46, 128.88, 128.12, 127.57, 125.76, 125.72, 120.62, 120.60, 120.51, 66.08, 54.89, 52.63, 47.14, 40.50, 39.24, 32.43, 31.75, 29.37, 27.11, 23.24, 22.79; ESI-MS for $C_{34}H_{41}N_{5}O_{5}$ [M+H] $^{+}$ calculated 600.3180; found 600.3189.

AAC peptides were sterilized by X-ray irradiation at 748 cGy/min for 30 min by RS 2000 irradiator (Rad Source Technologies; Suwanee, GA) that did not influence AAC structure.

2.1.2. Cells

2.1.2.1. Human visceral stromal vascular fraction (SVF) cells. Institutional review board–approved informed consent was obtained for the patients' medical records. Human visceral fat tissues (VF) were obtained from the greater omentum during endoscopic repair of hernias and/or bariatric surgeries (laparoscopic banding and gastric bypass) from overnight fasted in patients. Characteristic of subjects are described in Supplementary Table S1. Stromal vascular fraction cells (SVF) were isolated from VF using type 1 collagenase (Thermo Fisher Scientific, 17100017) following manufacture's instruction as described before [51]. Isolated cells were cultured in PGM-2 Preadipocyte Growth Medium-2 Bullet Kit (Lonza, PT-8002, supplemented with PT-9502; Basel, Switzerland). The medium was changed every 3 days prior to measurement of glucose uptake.

2.1.2.2. Human brain endothelial cells (hBEC). Human BEC were purchased from ATCC (CRL-3245). Cells were grown with DMEM:F12 (ATCC, 30–2006) supplemented with 10% FBS (Gibco, Gaithersburg, MD, 10082) and endothelial cell growth supplement (R&D systems, component of CCM027, Minneapolis, MN).

2.1.2.3. Mouse subcutaneous SVF cells. SVF cells were isolated from subcutaneous fat isolated from Lepr deficient mice (Homozygous for $Lepr^{db}$; 12-week old, JAX stock number 000642) or wild type male (C56BL6/J) using type 1 collagenase (Thermo Fisher Scientific, 17100017) following manufacture's instruction. The subcutaneous SVF cells were seeded in a flat 96-well plate in 100 μ L/well of high glucose DMEM (Gibco, 11965) supplemented with 10% FBS (Gibco, 10082) and 1% Penicillin-Streptomycin (10,000 U/mL; Gibco, 15140). Medium was changed every 48 h.

2.1.2.4. Mouse 3T3-L1 cells. Mouse 3T3-L1 fibroblast (preadipocyte) cells line were purchased from ATCC (CL-173).The 3T3-L1 preadipocytes were maintained in high glucose DMEM (Gibco, 11965) containing 10 % new born calf serum (Gibco, 26010) and 1% Penicillin-Streptomycin (10,000 U/mL; Gibco, 15140). Medium was changed every 48 h. Differentiation was initiated with medium containing 10% FBS, 1.7 μ M bovine insulin (Sigma I0516), 1 μ M dexamethasone (Sigma D4902), 0.5 mM 3-isobutyl-1-methyl xanthine (Sigma I7018). Medium was replaced every 48 h with DMEM containing 10 % FBS, 10 μ g/mL insulin, and continued for 6 days.

2.2. Animal studies

Animal studies were approved by the Institutional Animal Care and Use Committee of The Ohio State University (OSU). All mice were purchased from The Jackson Laboratory (Bar Harbor, ME) and were fed a regular chow diet (Teklad LM-485 mouse/rat diet, irradiated; Envigo,

Somerset, NJ) under 12 h:12 h light:dark cycle. Fasting glucose and body weight were monitored weekly. Mice were sacrificed by isoflurane inhalation followed by cardiac puncture.

2.2.1. LepR deficient mice (Lepr^{db})

The 5-week old male leptin deficient mice (Homozygous for $Lepr^{db}$; JAX stock number 000642) were randomly assigned to a control group treated with 10 μ L PBS/g body weight (BW) or AAC2 treatment (0.1 nmol/g BW). Six mice per group were used for this study. Nonfasted mice were injected subcutaneously into the scapular region every other day for 4 weeks.

2.2.2. Leptin deficient mice (Lep^{ob})

The 5-week old male leptin deficient mice (Homozygous for Lep^{ob} ; JAX stock number 000632) were randomized and treated as $Lepr^{db}$ mice (n = 5 per group).

2.2.3. Wild type mice

The aged male wild type mice (C57BL6/J; 37–38 week old) were fed a high fat diet (45% kcal from fat, Research Diets, D12451) to induce glucose tolerance. Mice were injected (i.p.) every other days with 10 μ L PBS/g BW (n = 5), AAC2 (0.1 nmol/g BW, n = 5) for 4 weeks.

2.2.4. Monogenic model for phenotypes associated with T1D

The 5 or 6-week old male C57BL/6- $Ins2^{Akita}$ /J (JAX stock number 003548) were injected intraperitoneally (i.p.) every other days with 10 μ L PBS/g BW, AAC2 (0.2 nmol/g BW), or hINS (1.7 nmol/g BW). Five mice per group were used for this study.

2.3. Methods

2.3.1. Transmission electron microscopy (TEM)

AAC1-AAC7 were dissolved in PBS to form 20 mM solution and left to self-assemble for 12 h. After gelation, the solution was diluted to 1 mM and 30 μ L diluted samples were loaded on the formvar/carbon-covered copper grid (Ted Pella, 01801, Redding, CA) and stained with uranyl acetate (1 wt% in distilled water) for 30 s and the grids were dried with filter paper. The nanostructures of the AAC1-AAC7 were observed by TEM (FEI Tecnai G2 Spirit, Thermo Fisher Scientific, Waltham, MA).

2.3.2. Critical micelle concentration of AAC2 with Nile Red

AAC2 samples were prepared by serial dilution starting from 2.5 mM in PBS with no aging. Nile Red (4.24 $\mu M,$ Acros Organics, NJ) was added and the solution was incubated for an additional 24 h. Fluorescence measurements were taken at excitation/emission 550 nm/656 nm, in a 3 mm quartz cuvette, slit widths 5, Cary Eclipse Spectrofluorometer (Agilent, Santa Clara, CA).

2.3.3. Quartz crystal microbalance with dissipation (QCM-D) binding assay Interaction of either AAC2 (0.1 μM in PBS) or mouse recombinant leptin protein (mLep; 1.6 fM in PBS; Crystal Chem, Elk Grove Village, IL, 90030-B) and with mouse recombinant leptin receptor (LepR) protein (1.6 pM in PBS; R&D systems, 497-LR/CF) were investigated by applying an alternating current on quartz via the piezoelectric effect using QCM-D [52,53]. We used quartz sensor with an active gold surface (QSX 301, Biolin Scientific, Sweden). The interaction of each component layer, measured as difference in frequency (ΔF) and dissipation (ΔD) values of the odd overtones was modeled using Voight-Voinova equations for homogenous viscoelastic layers [54,55].

2.3.4. Cell-based experiments and assays

2.3.4.1. Cytotoxicity test (WST-1 assay). 3T3-L1 preadipocytes were seeded into 48-well plates (5 \times 10^4 per well). Then, after 24 h, cells were treated with 0.1 μM AAC for 24 h in DMEM containing 10% calf serum. After incubation, 10 μl of WST-1 solution (Sigma-Aldrich, St. Louis, MO, 5015944001) was added directly into the media (1:10 ratio)

and incubated for 3 h. After incubation, absorbance was measured at 450 nm using Synergy H1 Hybrid Multi-Mode Microplate Reader (BioTek, Winooski, VT). Similar experiments were performed using different concentrations of AAC2 for 24 and 72 h in 3T3-L1 preadipocytes and hBEC cultures.

2.3.4.2. Detection of reactive oxygen species (ROS). ROS species production were detected using fluorescent CellROX Green Reagent (Thermo Fisher Scientific, C10444) according to manufacturer's instructions. 3T3-L1 preadipocyte cells were seeded into 48-well plates (5 \times 10^4 per well) and treated with 200 μ M $\rm H_2O_2$ (Sigma-Aldrich, H1009) for 4 h to induce cellular ROS production. After oxidative stress induction, these cells were treated with AACs (0.1 μ M each) and incubated for additional 24 h. Then, 5 μ M CellROX Green Reagent was used to stain live cell ROS accumulation by measuring absorption/emission maxima at 485/520 nm using fluorescence microscope. Quantification of ROS positive area was analyzed by ImageJ software (version 1.8.0_112).

2.3.4.3. Glucose uptake assay. General protocol. Glucose uptake was measured using fluorescent 2-deoxy-2-[(7-nitro-2,1,3-benzoxadiazol-4yl)amino]-D-glucose) (2-NBDG or FD glucose; Cayman Chemical, Ann Arbor, MI, 600470). For all experiments we used monolayer of cells. Cells were washed with PBS to remove residual glucose. Starvation conditions were induced in the DMEM medium, which does not contain glucose phenol red, and L-glutamine (Gibco, A14430, 200 μL /well) for 40 min otherwise described. The FD-working solution (0.29 mM) was prepared in the glucose-free medium. After treatment, cells were incubated with the FD-working solution containing reagents at 37°C for 80 min otherwise described. Cells were washed with PBS twice. Then, the fluorescence of cells was measured in cells containing 100 µL of PBS per well at an excitation/emission wavelength of 485/535 nm using Synergy H1 Hybrid Multi-Mode Microplate Reader (BioTek, Winooski, VT). The specifics of experimental conditions for each cell type are described below.

Human SVF were obtained from each donor and seeded at \sim 80% confluence on a flat-96 well plate in the 100 μL/well of PGM-2 Preadipocyte Growth Medium-2 Bullet Kit (Lonza, PT-8002, supplemented with PT-9502; Basel, Switzerland). After 3 days, glucose uptake was measured in confluent cells. The starved cells were stimulated with vehicle (Veh; PBS, Sigma-Aldrich, D8537), AAC2 (1, 3, 10, 30, and 100 nM for Fig. 2a; 0.03 μM for Fig. 2b) or AAC6 (1, 3, 10, 30, and 100 nM for Fig. 2a), or human insulin (hINS, 1.7 μM; Sigma-Aldrich, 19278) that were added into 100 μL of FD-working solution per well.

Experiment with PKC $_{\varsigma}$ inhibitor. Human visceral SVF cells were incubated with the ZIP inhibitor of a catalytic domain of PKC $_{\varsigma}$, which also exists as constitutively active form, i.e. protein kinase M $_{\varsigma}$ [56] (1 μ M; Abcam, UK, ab120993) or diluted in water or in glucose-free medium (Gibco, A14430) for 40 min. Then cells were incubated with Veh or AAC2 (0.1 μ M) in FD-working solution for 80 min.

Experiments with GLUT1 inhibitor. hBEC were split and seeded onto a 96-well plate (2 \times 10⁴/0.1 mL/well) coated with 0.1 % gelatin solution (Sigma-Aldrich, ES-006-B). After ~24 h, cells formed monolayer, then glucose uptake was performed. Cells were treated with vehicle (Veh; PBS, Sigma-Aldrich, D8537) or human insulin (hINS; 1.7 µM; Sigma-Aldrich, 19278) or human leptin (hLep; 62.5 nM, Thermo Fisher Scientific, RP-8634) or AAC2 (0.1 µM) which were diluted in same glucose free DMEM (Gibco, A14430, 200 µL/well) for 40 min. Then, GLUT1 inhibitor (BAY-876; 10 nM diluted in DMSO; Selleckchem, Houston, TX, S8452) or DMSO were added in 100 µL of FD-working solution per well and incubated for 50 min at 37 °C. 3T3-L1 preadipocytes were seeded in a 96 well plate at a density of 4×10^3 in 100 µL of culture medium per well and grow for 24 h prior to measurement of glucose uptake. Cells were pre-incubated with GLUT1 inhibitor (BAY-876; 10 nM diluted in DMSO) or DMSO diluted in DMEM not containing glucose phenol red, and L-glutamine (Gibco, A14430,

 $200~\mu L/well)$ for 40 min. Then, Veh or AAC2 (0.1 $\mu M)$ or human insulin (hINS; 1.7 $\mu M;$ Sigma-Aldrich, I9278) or mouse leptin (mLep; 12.5 nM, Peprotech, 450-31, Rocky Hill, NJ) were treated to cells with FD-working solution for 80 min.

Experiment with diverse AAC2 doses. 3T3-L1 cells were starved with glucose-free DMEM (Gibco, A14430) for 50 min. Then cells were treated with FD-glucose solution containing vehicle or AAC2 (10, 100, and 300 nM) for 100 min.

Experiment with anti-insulin receptor (InsR) antibody. 3T3-L1 cells were treated with heat-inactivated immunoglobulin or anti-InsR antibody (2.96 pM; EMD Millipore, Burlington, MA, MAB1137, LOT# 3010012) in glucose-free DMEM (Gibco, A14430). After 40 min incubation, cells were stimulated with Veh or AAC2 (0.1 μM) or human insulin (hINS; 1.7 μM ; Sigma-Aldrich, I9278) diluted in the FD-working solution for 80 min.

Experiment with PI3K and Akt inhibitors. 3T3-L1 cells were stimulated with FD-working solution containing AAC2 (0.1 μ M), PI3K inhibitor (Wortmannin, 0.1 μ M, Cayman Chemical, 10010591), pan-Akt inhibitor (GSK690693, 0.1 μ M, SelleckChem, S1113), or no reagents (Veh control) for 80 min.

Experiment with anti-leptin receptor (LepR) antibody. 3T3-L1 cells were treated with heat-inactivated immunoglobulin or anti-LepR antibody (3.2 pM; Thermo Fisher Scientific, PA1-28844, LOT# SH2429627A) in the glucose-free DMEM (Gibco, A14430, 200 μ L/well). After 40 min incubation, cells were stimulated with Veh or AAC2 (0.1 μ M) or mouse leptin (mLep; 1.6 fM in PBS; Crystal Chem, 90030-B) in the FD-working solution for 80 min. Similar experiment was performed using wild type subcutaneous SVF cells.

Subcutaneous mouse Lepr^{db} SVF cells were seeded in a flat 96-well plate and grown in high glucose DMEM (Gibco, 11965) containing 10% FBS (Gibco, 10082) and 1% Penicillin-Streptomycin (10,000 U/mL; Gibco, 15140) for 1 week. Cells were stimulated with FD working solution containing Veh or AAC2 (0.1 μ M), or mouse leptin (mLep; 12.5 nM, Peprotech, 450-31) for 80 min.

2.3.4.4. Western blot. Treated 3T3-L1 cells lysed using RIPA buffer (Thermo Fisher Scientific, 89900), containing Halt™ Protease and Phosphatase Inhibitor Cocktail (100X) (Thermo Fisher Scientific, 78440). Antibodies were purchased from Cell Signaling Technology (Danvers, MA): protein kinase B (PKB, alias: AKT, 4691S), phosphorylated (p-) p-AKT (9271S), signal transducer and activator of transcription 5 (STAT5, 94205S), p-STAT5 (4322S), STAT3 (9139S), the extracellular-signal-regulated kinase (ERK, 4696S), and p-ERK, (4370S). β-Actin was purchased from Sigma-Aldrich (A5441).

2.3.4.5. Protein concentrations. Protein concentrations were measured using Pierce BCA protein assay (Thermo Fisher Scientific, 23225).

2.3.5. Enzyme-linked immunosorbent assay (ELISA)

The level of mouse insulin was measured in mouse plasma by ELISA (EMD Millipore, EZRMI-13K) following the manufacturer's instruction. The absorbance at 450 and 590 nm were measured using Synergy H1 Hybrid Multi-Mode Microplate Reader (BioTek, Winooski, VT).

2.3.6. Glucose tolerance test (GTT)

GTT test was performed for all studies using 4–5 h fasted mice after 3 week treatment period. Mice were i.p. injected with 10 % glucose solution (w/v; 0.56 M, Gibco, 15023-021, diluted in distilled water and sterilized, 10 μ L/g BW). Glucose levels in tail-tip blood were measured using glucometer (OneTouch Ultra 2 m; LifeScan Inc., Milpitas, CA) during GTT experiments and weekly monitoring of glucose status.

2.3.7. Body composition measurement

Mouse body composition was measured with EchoMRI™-100H Body Composition Analyzer for Live Small Animals (EchoMRI™, Houston, TX) 4 weeks after treatment.

2.3.8. Comprehensive Lab animal monitoring system (CLAMS)

Metabolic parameters were measured by indirect calorimetry (CLAMS, Columbus Instruments, Columbus, OH) at an ambient temperature (22 °C) with 12 h light/dark cycles 7 weeks after treatment. Animals were fed the same diet and water provided ad libitum and consumption was measured. Mice were placed individually and metabolic parameters were measured for 24 h.

2.3.9. Open field test

The open filed test was performed at the Behavioral Core facility at OSU in blinded fashion using encoded groups of mice 5 weeks after treatment. Each animal is placed in a polypropylene open-field arena (36 cm \times 36 cm) with two rows of infrared sensors mounted on the sides to detect and distinguish between horizontal movements and vertical movements (Open Field Photobeam Activity System, San Diego Instruments, San Diego, CA). The arenas are contained in boxes that are light- and sound-attenuating. Activity counts are defined as interruptions in the infrared light sources by the animal (i.e., beam breaks). Total activity, amount of activity in the center versus the periphery of the arena, and number of rears is analyzed.

2.3.10. Barnes maze test

Barnes maze was performed as described in Ref. [57]. The Barnes maze, (122 cm diameter) with 18 escape holes (9.5 cm) placed every 20° around the perimeter (ENV-563-R, MedAssociates, St. Albans, VT, USA), was surrounded with a 60 cm high white polycarbonate barrier to prevent escape. The blind escape holes were blocked by black panels, and the target escape hole was visually the same as the blind holes, but contained a black escape box (38.7 \times 12.1 \times 14.2 cm). Distinct visual cues (black 2 dimensional geometric shapes, 20-25 cm) on the upper edge were attached to of the surround at the 4 compass points and present visual cues distal to the maze. Testing consisted of 5 days of acquisition training followed by a single probe trial 24 h after the last training trial. Each acquisition day consisted of one session/animal, 3 trials per session, with an inter-trial interval of 5 min. For acquisition training, all mice were allowed to acclimate for 30 min before the start of testing. Each trial consisted of carefully placing the mouse in the center of the maze from the opaque plastic beaker. The mouse was allowed to search for the escape box for 120 s, then it was guided to it. Olfactory cues were eliminated by cleaning with 70% ethanol after testing of each mouse, and each day the maze was rotated 90° counter clockwise, with the escape box location and location of visual cues remaining constant throughout testing. All behavior on coded mice were recorded and scored using The Observer software (XT 8.0; Noldus, Leesburg, VA, USA). For training trials, latency to escape and number of errors were recorded. An error was defined as an investigation of a blind escape hole where the entire head of the mouse broke the plane of the edge of the escape hole. For the probe trial, latency to escape hole, number of errors, and time in quadrant of escape hole (% in path Q3) were measured.

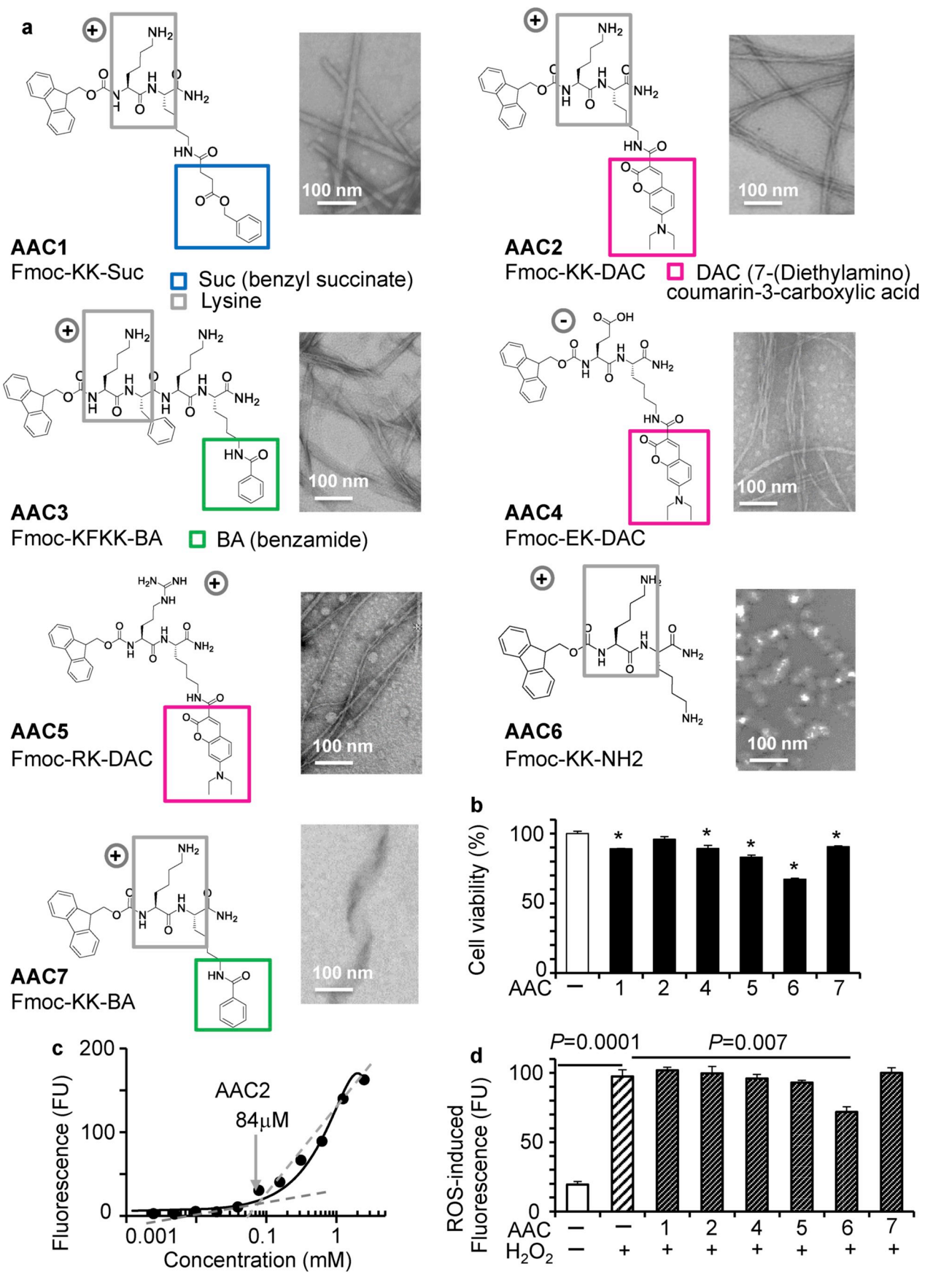
2.3.11. Statistical analysis

All data were analyzed using SPSS 23 (IBM Corp., Armonk, NY). All data are shown as mean \pm standard error (SEM). Number of samples for each assay is indicated in Figure legends. Group comparisons were assessed using Student's independent or paired t-test (two-sided) or oneway analysis of variance (ANOVA) for normally distributed samples. Mann-Whitney U test or Kruskal-Wallis test were used as nonparametric tests. P < 0.05 was considered statistically significant.

3. Results

3.1. Amino acid compounds regulate glucose uptake in vitro

Given the glycemic properties of lysine and coumarin class of compounds [48], we specifically incorporated 7-(diethylamino)



(caption on next page)

Fig. 1. Structure, physical characteristics, cytotoxicity, and antioxidant properties of seven Amino Acid Compounds (AAC 1–7). (a) Chemical structures of seven amino acid compounds (AAC). Self-assembled nanostructures of AAC (1 mM) were imaged by transmission electron microscopy (TEM) at 225,000 magnification. Grey box indicated backbone amino acid structure responsible for the charge of molecule. The blue, red, and green boxes represent specific site moiety for the AAC molecules. (b) Cytotoxicity was measured in 3T3-L1 preadipocytes treated with AAC compounds (0.1 μ M, black bars) or left untreated (white bar) for 24 h (n = 4 per treatment condition). Viable cells were quantified using WST-1 assay. Data are shown as % of control. Asterisk, P < 0.05 compared to control, Student's independent t-test. (c) Assembly of AAC2 into micelle (nanofibers) was measured by monitoring the fluorescence of the lipophilic dye Nile Red in the presence of AAC2 at different concentrations. An arrow shows the critical micelle concentration. (d) Reactive oxygen species concentration was measured in 3T3-L1 preadipocytes stimulated with H_2O_2 for 4 h (200 μ M, hatched bars) and treated with and without (open bar) AAC (0.1 μ M dark hatched bars) for 24 h. ROS-induced fluorescence was measured using CellROX Green Reagent. Student's independent t-test, n = 3/condition.

coumarin-3-carboxamide as a peptide side-chain (Fig. 1a). To explore the potential of small, lysine-containing peptides to serve as more potent antidiabetic drugs, we designed and tested a series of peptides termed amino acid compounds (AAC) that varied several structural elements. The series probed the impact of peptides with positive charge (AAC1-AAC3, AAC5-AAC7), negative charge (AAC4), and coumarin side-chains (AAC2, AAC4, and AAC5) on antidiabetic efficacy (Fig. 1a, Fig. S1). To ascertain the importance of the coumarin side-chain for activity, benzyl succinate (AAC1), and benzamide derivatives (AAC3 and AAC7) were also studied. All of these AAC peptides, with the exception of AAC6, have potential to undergo a concentration-dependent self-assembly into nanofibers under physiological conditions in PBS [58].

We examined short (6 h) and long-term (24 h) toxicity of AAC compounds on murine 3T3-L1 fibroblasts. AAC3 exhibited a significant toxicity within 6 h and was excluded from further experiments (Fig. S2). Low but significant toxicity was seen in the presence of AAC1 and AAC4-7 after 24 h incubation (Fig. 1b). The cell viability was identical in control and AAC2-treated cells. We increased the AAC2 concentrations and examined their effects on viability of fibroblasts and also human brain endothelial cells for the prolonged (24–72 h) period of time (Fig. S2 b,c). AAC2-treated cells of both types have similar viability as control cells 24 h after the beginning of experiments. Overall, these experiments suggest the lack of AAC2 toxicity in peripheral and brain cells.

At the exceptionally low concentrations used in this study, the AAC2 peptides remained in monomeric form. For example, the critical micelle concentration, as measured by Nile Red encapsulation, was 84 μM for AAC2, which was 840 times higher than the concentrations used for the cell cultures (Fig. 1c). The dilution of preformed AAC2 nanofibers at 1 mM concentrations led to their immediate and stable dissociation (Fig. S3). Therefore, in all biological studies, we characterized the properties of the monomeric AAC2 form.

Since the lysine side-chains were derivatized with potential antioxidants, we also examined antioxidant properties of AACs under oxidative stress conditions induced by hydrogen peroxide (Fig. 1d). Among all AAC compounds, only AAC6 reduced reactive oxygen species production in the presence of hydrogen peroxide; however, the toxicity profile of AAC6 was higher than that of AAC2. We proceeded with both AAC2 and AAC6 for testing of glycemic properties, the primary selection criteria for the in vitro studies.

We followed guidelines to de-risk safety and efficacy [59] by performing experiments with human tissues to assess the relevance of our findings for humans. We selected the relevant primary human stromal vascular fraction preadipocytes (SVF) for testing glucose uptake, because insulin resistance in visceral fat is a key risk factor for insulin resistance and T2D [13,18,60]. These cells were isolated from visceral (omental) fat from obese patients (Supplementary Table S1) undergoing surgeries and serve as an example of a peripheral tissue. AAC2 stimulation lead to a dose-dependent increase in glucose uptake in SVF preadipocytes, in contrast AAC6 reduced glucose uptake in same cells (Fig. 2a). Thus, only AAC2 could regulate glucose uptake in vitro. Based on two primary selection criteria, such as the absence of toxicity and efficacy in glucose uptake, AAC2 was selected as a candidate molecule for investigation of its glycemic effects.

Next, we compared AAC2 and human insulin (hINS) effects on

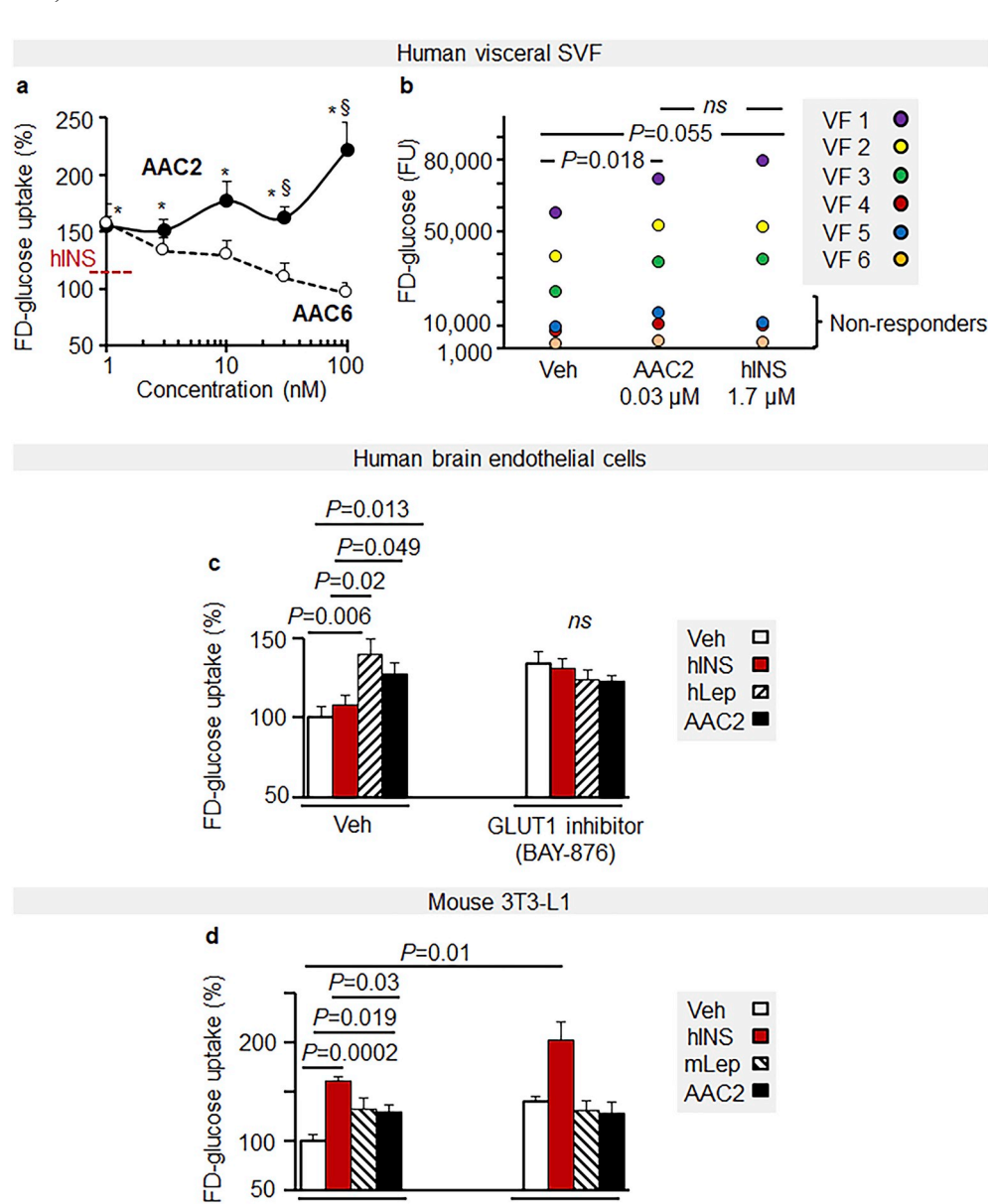
glucose uptake and SVF isolated from six patients. AAC2 significantly stimulated glucose uptake in all patients, whereas hINS showed a trend (P = 0.055) for increasing glucose uptake (Fig. 2b). SVF preadipocytes for 50% of obese patients were not responding to insulin stimulation; however, these cells have increased glucose uptake in the presence of AAC2. We further investigated the glycemic properties of AAC2 in human brain endothelial cells (hBEC), which utilize primarily GLUT1 [61]. In these cells only AAC2 and leptin induced glucose uptake, which was abolished by GLUT1 inhibitor (Fig. 2c). Insulin did not influence glucose uptake in hBEC cells. We performed a similar experiment in mouse 3T3-L1 preadipocytes expressing GLUT4 as a major transporter and GLUT1 as a minor transporter [2]. Insulin, AAC2, and leptin all induced significant glucose uptake in 3T3-L1 preadipocytes (Fig. 2d). The inhibition of GLUT1 with BAY-878 inhibitor abolished glucose uptake by AAC2 and leptin, but not insulin. The glucose uptake was not limited to preadipocytes. Differentiated 3T3-L1 adipocytes increased glucose uptake in response to different doses of AAC2 but were more resistant to leptin and insulin stimulation in adipocytes vs. preadipocytes in agreement with insulin and leptin resistance phenomena (Fig. S4). Together, these data demonstrate that AAC2 and leptin mediate glucose transport in human and animal cells using different transporters than insulin. AAC2 efficiently mediated glucose uptake in peripheral adipocytes and in endothelial cells of nervous tissue.

3.2. AAC2 regulates glucose uptake via LepR and PKC5

We performed studies in 3T3-L1 preadipocytes to determine a mechanism of AAC2-mediated glucose uptake. AAC2 increased glucose uptake in a dose-dependent manner in 3T3-L1 preadipocytes (Fig. 3a). Both hINS and AAC2 stimulations induced significant uptake of glucose compared to non-stimulated 3T3-L1 cells (Fig. 3b). In line with the previous reports, IgG antibodies increased basal glucose uptake [62]. Nonetheless, the pretreatment of these cells with the anti-insulin receptor (InsR) antibodies blocked glucose uptake mediated by hINS, but not by AAC2. To strengthen this initial observation, we analyzed contribution of classic AKT and PI3K pathways that mediate downstream effects of activated InsR in 3T3-L1 preadipocytes [63]. Inhibition of AKT and PI3K did not influence AAC2-mediated glucose uptake in these cells (Fig. 3c) suggesting that AAC2 and insulin act via different pathways. We also ruled out that AAC2-mediated glucose uptake is regulated by various other pathways (Fig. S5), since inhibition of AMPK and MAPK, PPARα, as well as EGFR and FGFR pathways did not prevent the increase in glucose uptake in the presence of AAC2.

Glucose uptake in peripheral tissues depends on leptin activation of LepR pathway [19]. We compared glucose uptake mediated by AAC2 or leptin in 3T3-L1 preadipocytes pretreated with inactivated or intact antibodies against LepR (anti-LepR Fig. 3d). Inhibition of LepR by anti-LepR antibodies prevented glucose uptake mediated by either AAC2 or leptin in 3T3-L1 preadipocytes. We validated this response in primary SVF cells isolated from visceral fat of *Lepr*^{db} mouse with a dysfunctional mutant LepR (Fig. 3e) as well as primary SVF cells isolated from WT mice (Fig. S6). In these cells with genetically dysfunctional LepR, leptin and AAC2 were unable to activate glucose uptake. These data indicate that leptin and AAC2 act via LepR.

Next, we compared the major signaling pathways mediated by exposure of 3T3-L1 cells to insulin, leptin, and different doses of AAC2 for



(%) was normalized to FD-glucose uptake in control (Veh) 3T3-L1 cells without inhibitor (100%). Student's independent *t*-test. . (For interpretation of the references to colour in this figure legend, the reader is referred to the Web version of this article.)

GLUT1 inhibitor

(BAY-876)

5 min (short-term) and 15 min (Fig. 3f). In these cells representing peripheral tissues, insulin acted in classical manner inducing phosphorylation of AKT in a time-dependent manner. Insulin stimulation also led to a weak, late phosphorylation of mTOR, STAT3, STAT5, and ERK after 15 min treatment. Leptin induced phosphorylation of STAT5 and ERK after 15 min 3T3-L1 stimulation. Short-term stimulation with leptin only resulted in phosphorylated mTOR. AAC2 only moderated transient effects on phosphorylation of AKT, mTOR, STAT3, or STAT5 (quantified data in Figs. S7a-d). AAC2 stimulation increased in a dosedependent and time-dependent manner phosphorylation of ERK and atypical PKCs Figs. S7e and f). PKCs has been previously proposed to mediate glucose uptake in response to mechanical stretch in muscle cells [64]. We examined the role of PKCs in the regulation of AAC2mediated glucose uptake in 3T3-L1 cells (Fig. 3g). The catalytic domain of PKC can exist also as protein kinase Mg (PKMg) in the nervous and possibly other tissues [56]; therefore, we used a ZIP inhibitor to inhibit catalytic activities associated with PKCs. ZIP has no effect on glucose uptake in control cells; however, it abolished AAC2-mediated glucose

Veh

uptake (Fig. 3g). These data provide additional evidence indicating that AAC2 signals in a different manner than leptin via PKC ς with or without PKM ς to mediate glucose uptake.

Fig. 2. AAC2 induced glucose uptake in

adipocytes and brain endothelial cells

(hBEC) in GLUT1-dependent manner in

vitro. (a) Dose-dependent FD-glucose up-

take in SVF cells stimulated with AAC2

(closed circles) and AAC6 (open circle). SVF were collected from an individual donor. Data (n = 8 per treatment) was normalized

to FD-glucose uptake in non-stimulated cells

(% compared to Veh). Red dashed line

shows FD-glucose uptake cells stimulated

with human insulin (hINS; 1.7 µM).

Student's independent t-test. Asterisks,

P < 0.05 compared to Control (PBS). §,

P < 0.05 comparison between AAC2 vs. AAC6. (b) FD-glucose uptake in non-treated (Veh) SVF cells or stimulated with AAC2

(0.03 $\mu M),$ or hINS (1.7 $\mu M)$ for 80 min. SVF were isolated from 6 different subjects

(circles, Supplementary Table 1) Data are

shown as mean ± SEM of fluorescence

units (FU) from n = 8/subjects/treatment.

Student's paired t-test. (c) FD-glucose up-

take in human brain endothelial cells

(hBEC, n = 8 per treatment) treated with

vehicle (Veh; PBS, open bar) or hINS

(1.7 µM, red bar), human leptin (hLep;

62.5 nM, hatched bar), or AAC2 (0.1 μ M black bar) in the presence and absence of GLUT1 inhibitor (BAY-876; 10 nM in DMSO). Cells were pre-treated with or

without BAY-876 for 40 min and then FD

glucose and treatment reagents were added for additional 50 min of incubation. Data

(%) was normalized to FD-glucose uptake in control (Veh) hBEC without inhibitor

(100%). Student's independent *t*-test. *ns*, not significant. (d) FD-glucose uptake in mouse

3T3-L1 preadipocytes (n = 8 per treatment)

treated with vehicle (Veh; PBS, open bar) or

hINS (1.7 μM, red bar), mouse leptin (mLep;

12.5 nM, hatched bar), or AAC2 (0.1 μM

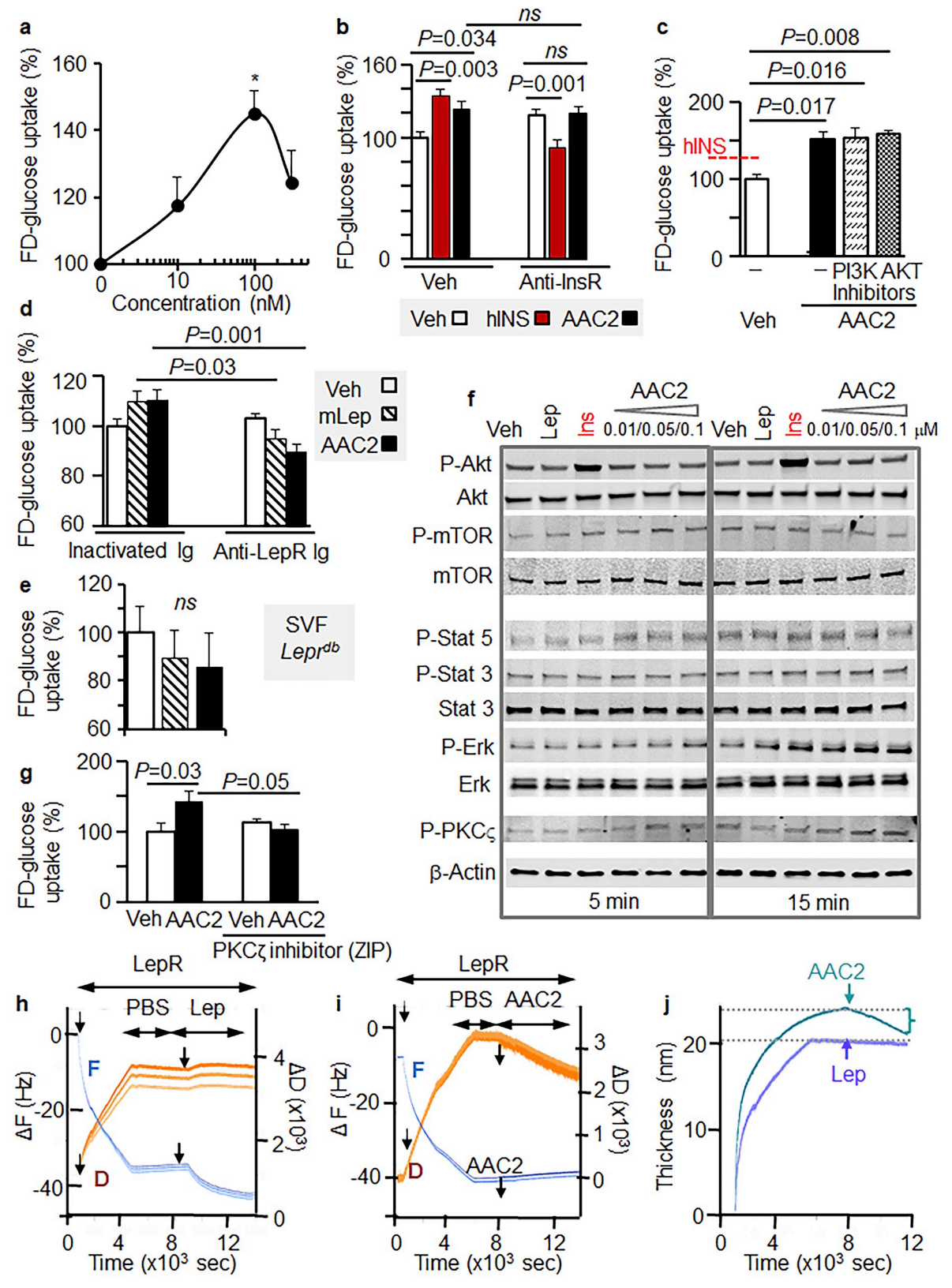
black bar) in the presence and absence of GLUT1 inhibitor (BAY-876; 10 nM in

DMSO). Cells were pre-treated with or

without BAY-876 for 40 min and then FD glucose and treatment reagents were added

for additional 80 min of incubation. Data

To compare the molecular interaction between LepR and its canonic ligand leptin (Fig. 3h) as well as the interaction of AAC2 with LepR (Fig. 3i), we used a quartz crystal microbalance. The binding of LepR increased the dissipation and decreased the frequencies associated with the active gold surface (Fig. 3h). The binding of leptin further increased the dissipation and decreased the frequencies seen with LepR, indicating formation of the film on the gold surface (Fig. 3h). In contrast, the interaction of AAC2 led to the release of the LepR from the active gold surface due to the formation of AAC2/LepR complex (Fig. 3i). This effect was evident as the decreased dissipation and the increased frequencies after AAC2 addition compared to those seen with LepR alone (Fig. 3i). Consequently, the thickness of the LepR film was decreased after interaction with AAC2, but was not altered after canonical binding of leptin (Fig. 3j). The interaction between AAC2 and LepR was strong, albeit principally different from the binding of leptin. Evidently,



(caption on next page)

Fig. 3. Glucose uptake mediated by AAC2 depends on LepR and PKCs in vitro. (a) Dose-dependence FD-glucose uptake stimulated by AAC2 in 3T3-L1 preadipocytes after 100 min of incubation (n = 6 per dose). Data were normalized to FD-glucose uptake (%) in control (Veh 100%). Asterisk: P = 0.019, Student's independent t-test. (b) FD-glucose uptake in non-stimulated (Veh, open bar) or stimulated with AAC2 (0.1 µM, black bar) or hINS (1.7 µM, red bar) in 3T3-L1 cells for 80 min. Prior to stimulation cells were pre-treated with Veh, heat-inactivated immunoglobulin (data not shown), or anti-InsR antibody (2.96 pM) for 40 min. Data were normalized to FD-glucose uptake (%) in control (Veh 100%). Student's independent t-test. ns, not significant. (n = 8 per treatment). (c) FD-glucose uptake (%) vs. Veh; n = 8) in presence of AAC2 (0.1 µM) with and without PI3K inhibitor (Wortmannin, 0.1 µM), or pan-Akt inhibitor (GSK690693, 0.1 µM) in 3T3-L1 preadipocytes. Human insulin (hINS; 1.7 µM) was used as a positive control (red dashed line, n = 8). One-way ANOVA with Bonferroni's post hoc test. P = 0.003 for overall comparisons among treatments. (d) FD-glucose uptake (% compared to Veh; n = 8) in presence of AAC2 (0.1 μM) or recombinant mouse leptin protein (12.5 nM) in 3T3-L1 preadipocytes pretreated with inactivated antibodies or polyclonal anti-LepR antibodies (3.2 pM). Two-sided paired t-test for each condition. (e) FD-glucose uptake (% compared to Veh; n = 8) in presence of AAC2 (0.1 µM) or recombinant mouse leptin protein (0.01 µM) in SVF cells isolated from subcutaneous fat of Lepr^{db} mouse. Kruskal Wallis test. P = 0.418 for overall comparison (not significant, ns). (f) Expression of phosphorylated and non-phosphorylated proteins was measured in 3T3-L1 preadipocytes stimulated with indicated compounds for 5 or 15, minutes using Western blot. (g) FD-glucose uptake (% compared to Control; n = 8) in presence in the absence (Veh, open bar) of AAC2 (0.1 μM, black bar) in human visceral SVF cells with and without ZIP inhibitor of catalytic domain of PKCc/PKMc (1 µM). Cells were pretreated with ZIP inhibitor for 40 min and treated with reagents and FD-glucose for 80 min. Student's independent t-test (n = 8 per treatment). (h, i) Binding affinity of recombinant mouse leptin receptor protein (LepR) and leptin (h) or binding affinity between LepR and AAC2 (i) were analyzed with QCM-D. Arrows indicate the starting point of addition of each reagent. Blue line shows frequency (F). Red line shows dissipation (D). (j) Thickness of LepR-Leptin film or LepR-AAC2 film was quantified based on the binding kinetics in (h,i). (For interpretation of the references to colour in this figure legend, the reader is referred to the Web version of this article.)

atypical AAC2 binding to LepR mediated different PKC ς signaling leading to increased uptake of glucose in vitro.

We examined the dependence of AAC2 effects on LepR *in vivo* in Lepr^{db} mice treated with AAC2 for one month. Activation of LepR regulates glucose uptake, food intake, weight, and insulin secretion [65,66]. AAC2 did not improve any of these functions in Lepr^{db} mice. A glucose tolerance test (GTTs) showed that AAC2 treatment impaired glucose uptake compared to non-treated Lepr^{db} mice (Fig. 4a). AAC2

treatment had no effect on food intake (Fig. 4b), weight gain (Fig. 4c), or insulin levels (Fig. 4d) in *Lepr*^{db} mice. In contrast, similar AAC2 treatment improved glucose uptake in WT mice treated with AAC2 for one month (Fig. S8).

The interaction of AAC2 with LepR was also examined in Lep^{ob} mice expressing LepR but deficient in leptin, a natural ligand for this receptor. Lep^{ob} mice were treated with AAC2 under a similar regimen as $Lepr^{db}$ mice. AAC2 treatment markedly improved glucose tolerance in

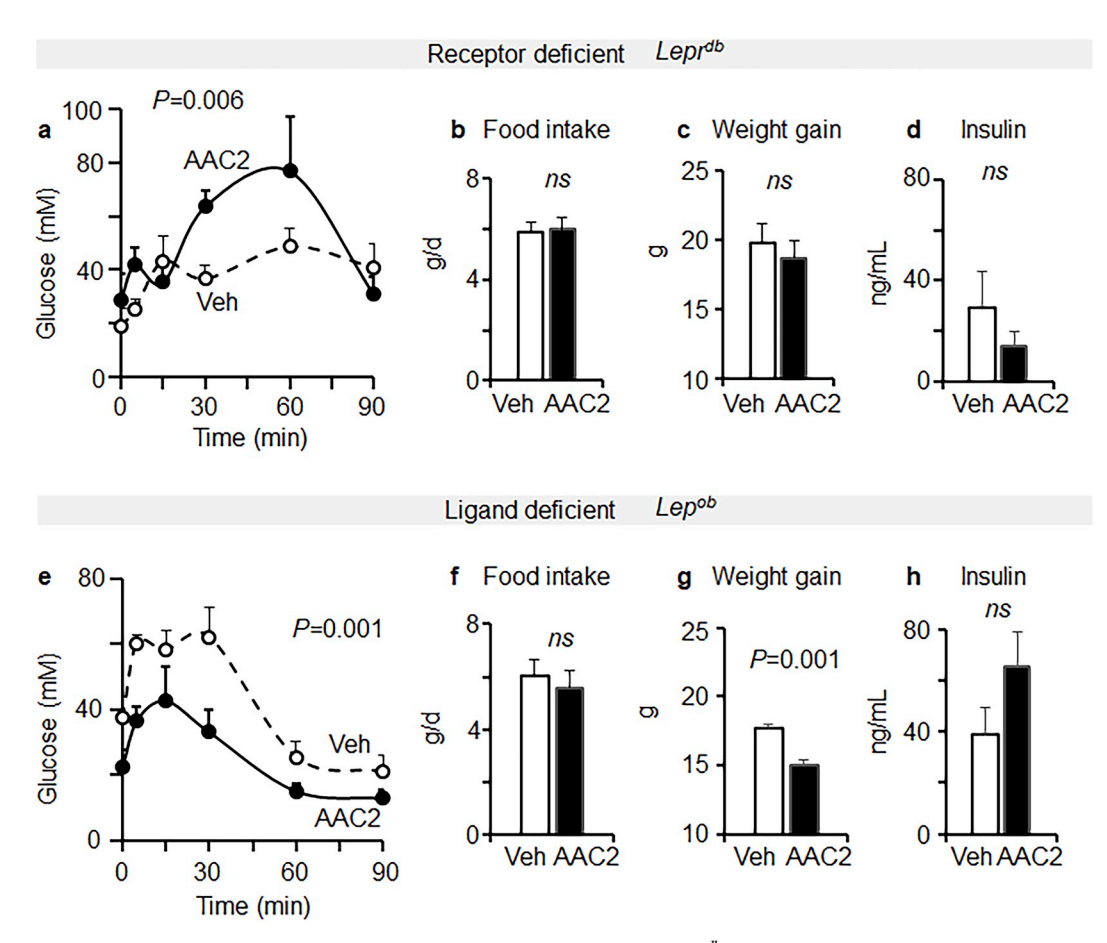


Fig. 4. AAC2 induced glucose uptake by LepR-dependent mechanism in vivo. (a) GTT in $Lepr^{db}$ mice treated without (Veh, open circles, n=6) or with AAC2 (black circles, n=6). Student's independent t-test for each time point. P=0.006 at 30 min post glucose injection. (b,c) Food intake, P=0.817, ns. (b) and weight gain P=0.576, ns. (c) in $Lepr^{db}$ mice treated without (Veh, open bars, n=6) or with AAC2 (black bar, n=6). (d) Insulin levels in plasma of same $Lepr^{db}$ mice were measured by ELISA. P=0.416, ns. (e) GTT in Lep^{ob} treated without (Veh, open circles, n=5) or with AAC2 (black circles, n=5). Student's independent t-test for each time point. P=0.001 and P=0.045 at 5 min and 30 min post glucose injection, respectively. (f-h) Food intake, P=0.133, ns. (f), weight gain (g), and insulin levels (h) in Lep^{ob} mice treated without (Veh, open bar, n=5) or with AAC2 (black bar, n=5) P=0.17, ns. Student's independent t-test.

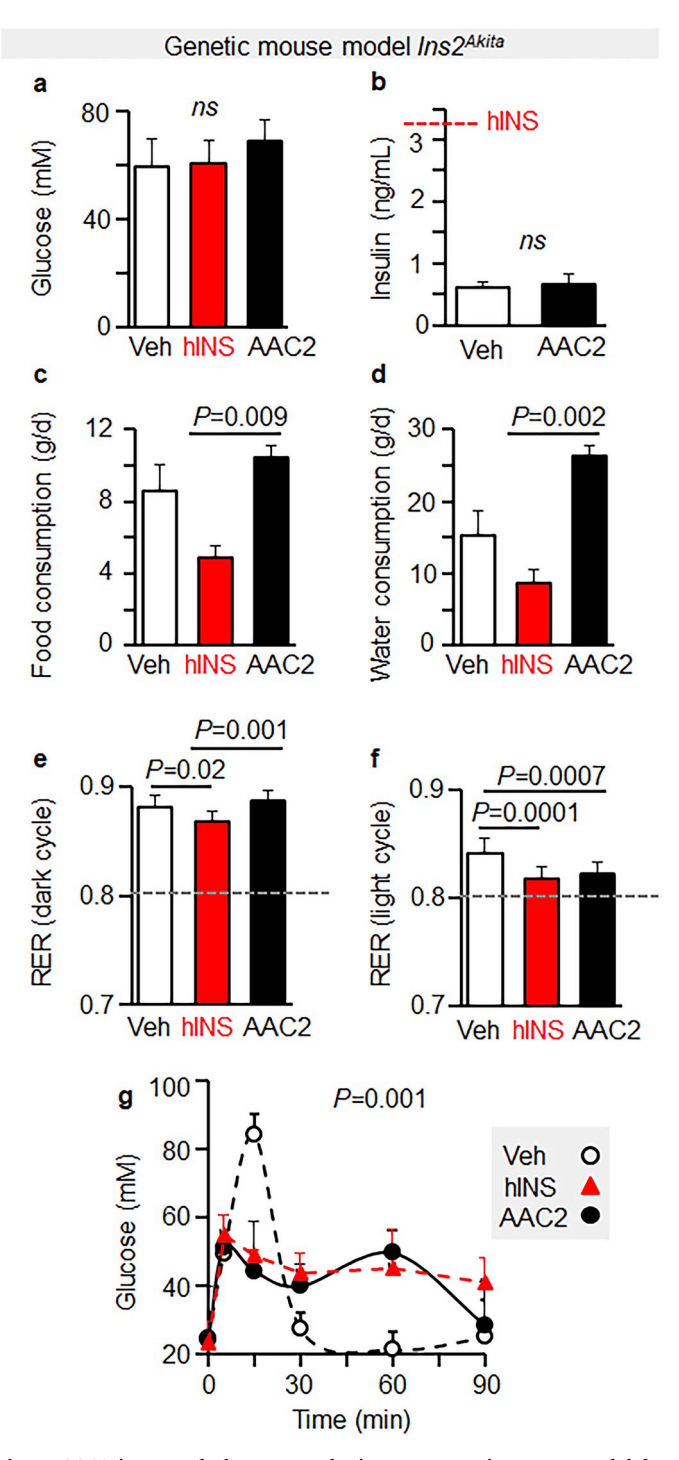


Fig. 5. AAC2 improved glucose uptake in a monogenic mouse model for phenotypes associated with insulin deficient T1D. (a) Baseline fasting glucose levels prior to treatment in $Ins2^{Akita}$ mice (n = 5 per group). Kruskal Wallis test, P=0.908 for overall comparison (ns, not significant). (b) Mouse insulin levels measured in same $Ins2^{Akita}$ mice at the end of the study. Student's independent t-test. P=0.720 (ns, not significant). (c, d) Food and water consumption measured in same $Ins2^{Akita}$ mice 7 weeks after treatment using CLAMS. Student's independent t-test. (e, f) Respiratory exchange ratio (RER) measured in same $Ins2^{Akita}$ mice during the dark (e) and light (f) period using CLAMS measurements of O_2 use and CO_2 production. Student's independent t-test. (g) GTT was performed in same $Ins2^{Akita}$ mice 3 weeks after beginning of treatment. One way ANOVA.

 Lep^{ob} mice (Fig. 4e) suggesting that the glycemic action of AAC2 compensated for the absence of leptin. Although the decrease in food intake in AAC2-treated Lep^{ob} mice did not reach statistical significance (Fig. 4f), these mice gained significantly less weight compared to control mice in agreement with the known responses of activated LepR (Fig. 4g) after one month of treatment. The insulin levels were not statistically different in AAC2-treated and control mice (Fig. 4h). Therefore, AAC2 did not replicate all effects of leptin (Fig. 4), which is in consonance with the specific mechanism underlying the interaction of this compound with LepR (Fig. 3d, e, h-j). The studies in Lep^{ob} in $Lepr^{db}$ mice demonstrate that AAC2 effectively regulates glycemic effects in the absence of leptin and LepR is required for these action (Fig. 4).

3.3. AAC2 improved glucose uptake in genetic models of T1D without insulin

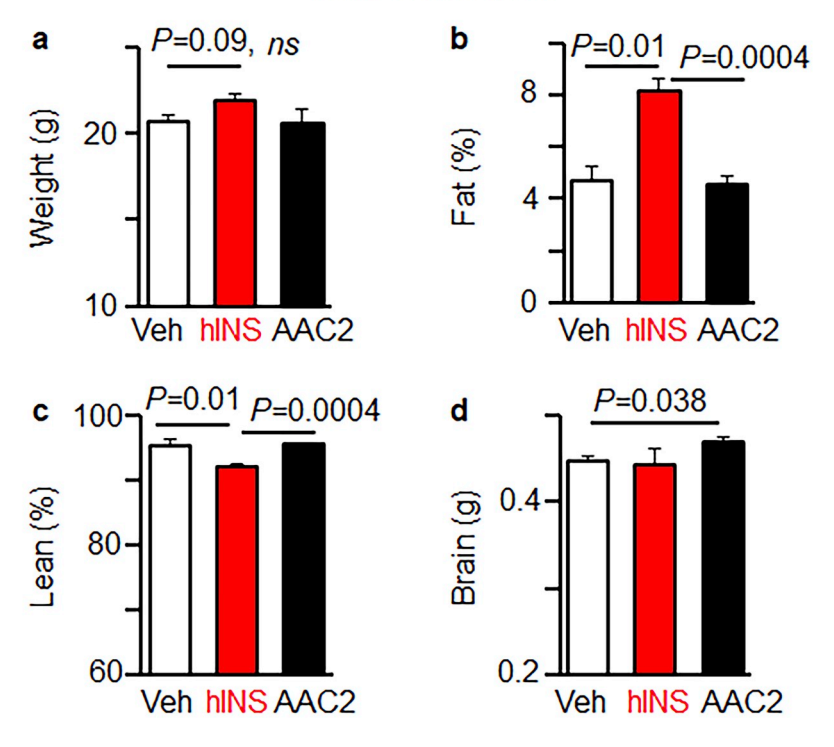
Given the unique mechanism of glycemic AAC2 function, we tested the efficacy of this compound in a genetic model of deficient insulin signaling. An established monogenic model of T1D is a heterozygous Ins2^{Aktia} mice [67]. Mutation in Ins2 gene in these mice lead to production of misfolded INS2 that leads to autoimmune destruction of pancreatic β -cells [68]. Five week old male $\mathit{Ins2}^{\mathit{Akita}}$ mice developed severe hyperglycemia (Fig. 5a) that was consistent with criteria for T1D (fasting glucose > 13.9 mM [69]) and published data [68]. After these severly hyperglycemic mice were randomized in an untreated control and three experimental groups treated with hINS or AAC2 for 4 weeks. Mice were injected every 48 h. Control group and AAC2-treated mice have similar levels of insulin in circulation after 4 weeks for treatment, whereas the level of insulin was higher in hINS-treated mice (Fig. 5b). Mice treated with AAC2 or hINS exhibited different food and water consumption that were measured in the individually housed mice in metabolic cages (Fig. 5c and d). AAC2-treated mice consumed more food (Fig. 5c) and water (Fig. 5d) compared to hINS-treated mice. Regulation of both food [65] and water [70] consumption has been attributed to the activation of LepR in hypothalamus in the previous

In spite of the differences in food and water consumption all mouse groups exhibited a respiratory exchange ratio (RER) higher than 0.8 during active dark and light day cycles, suggesting that they all utilized glucose as the primary energy substrate (Fig. 5e and f). Mice treated with hINS or AAC2 showed a circadian pattern of RER regulation that was significantly reduced during the resting light cycle (Fig. 5f). GTT revealed severe glucose tolerance in control $Ins2^{Akita}$ mice reaching maximum at > 80 mM glucose concentration in blood (Fig. 5g). AAC2 and hINS treatments markedly improved systemic glucose uptake in $Ins2^{Akita}$ mice with comparable efficacy (Fig. 5g). Thus, AAC2 mimicked the potency of hINS in the regulation of glucose uptake in genetic mouse model of T1D.

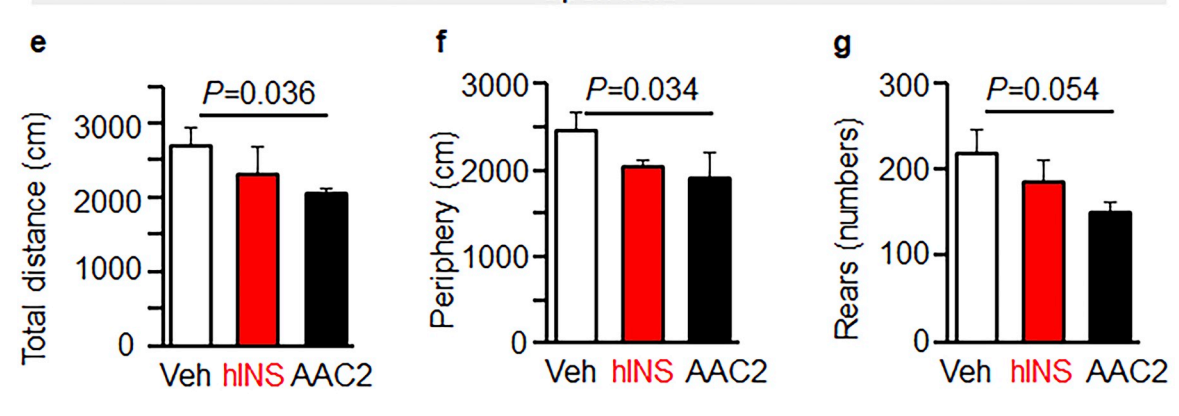
3.4. AAC2 improves body composition and anxiety response in Ins2^{Akita} mouse model of T1D

Although both hINS and AAC2-treated *Ins2*^{Akita} mice demonstrated similar glucose uptake, they imposed a different impact on the body composition of the mice. All *Ins2*^{Akita} mice had similar weights at the end of the study (Fig. 6a). However, the proportion of fat was 172% higher in hINS-treated mice compared to control *Ins2*^{Akita} mice or mice treated with AAC2 (Fig. 6b). The paradoxical increase in adiposity associated with decreased food consumption has been previously described by other researchers in insulin-deficient mice [15]. As an anabolic hormone, insulin induces lipogenesis and increases adiposity in

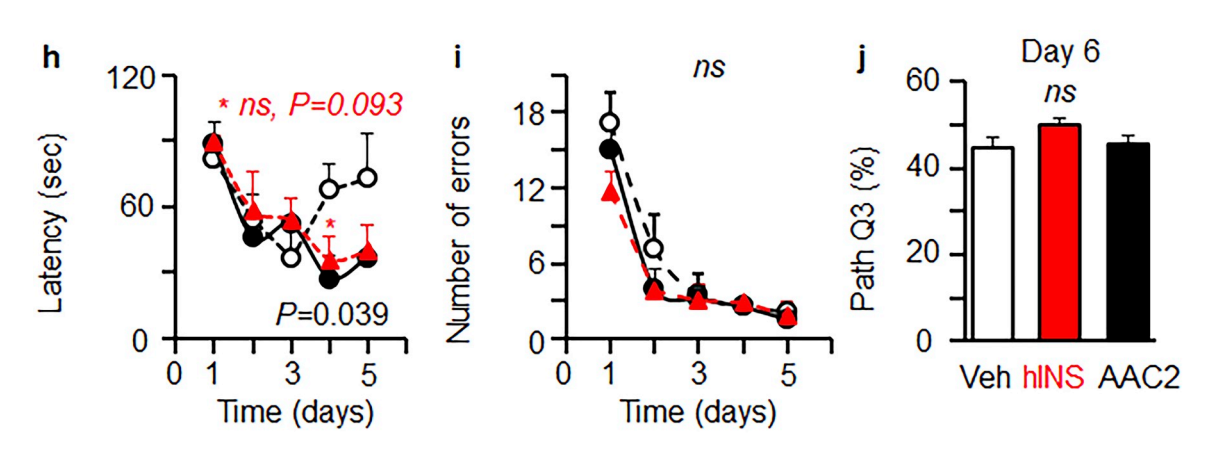
Body composition







Barnes maze



(caption on next page)

Fig. 6. AAC2 and insulin have different impact on body composition associated with decreased anxiety like behavior in $Ins2^{Akita}$ mice. (a–c) Body weight (a), percent body fat (b), and percent lean body mass (c) were measured in $Ins2^{Akita}$ mice (n = 5 per group) 4 weeks after treatment using EchoMRITM-100H Body Composition Analyzer. Student's independent t-test. ns, not significant. (d) Brain weight in same $Ins2^{Akita}$ mice was measured at sacrifice. Student's independent t-test. (e–g) Total movement distance (e), amount of activity in the periphery of the arena (f), and number of rears (g) was conducted using open field test $Ins2^{Akita}$ mice 5 weeks after treatment. Student's independent unpaired t-test. (h,i) Barnes Maze test was performed with $Ins2^{Akita}$ mice after 7 weeks post-treatment (n = 5 Veh, n = 5 AAC2, n = 5 hINS). In the training period (Day 1–5), latency (h) and number of errors (i) were measured. Differences were compared for each day by Student independent t-test. Significantly differences between control and AAC2-treated mice on day 4 are shown, the difference between control and hINS-treated mice on day 4 was not significant (n.s.). (j) Hole escape time at day 6 (Q3 in same experiment). Kruskal Wallis test with a Mann-Whitney U test for post hoc testing, the differences were not significant.

patients with T1D and in animal models of this disease [14]. Correspondently, hINS-treated *Ins2*^{Akita} mice in our study had reduced the proportion of lean mass to whole body mass (Fig. 6c). Thus, AAC2 acted different than insulin. In contrast, AAC2-treated mice had a similar composition of fat and lean mass as the control group (Fig. 6d). Importantly, AAC2-treated mice had significantly higher brain mass compared to the control group (Fig. 6d). The difference in brain mass between hINS-and AAC2-treated mice was not statistically significant. To understand the functional relevance of the changes in brain mass, we performed a behavioral open field test to assess locomotor activity levels, anxiety, and exploration habits [71]. Distance traveled in the light compartment was 24 % shorter in AAC2-treated mice compared to control Ins2Akita mice (Fig. 6e). AAC2-treated mice spend significantly reduced amount of time in periphery than control Ins2Akita mice (Fig. 6f). The time spent in the periphery was similar between the hINS and AAC2-treated Ins2Akita mice. AAC2-treated mice exhibited significantly reduced number of rears, suggesting reduced anxiety like behavior (Fig. 6g).

We also assessed spatial learning and examined the cognitive performance using Barnes maze test [57] (Fig. 6h–j). The latency period (time required to find the escape box, maximum of 120 s) was significantly shorter in the group treated with AAC2 (27 s) compared to control group (67.3 s); whereas the improvement in hINS treated mice (35.9 s) was not statistically significant (Fig. 6h). The $Ins2^{Akita}$ mice treated with hINS or AAC2 made a similar amount of errors in spatial orientation compared to the control group (1.5 AAC2,1.9 hINS vs. 2.1 errors in control) at the end of the training period (Fig. 6i). The acquisition and retention of the spatial reference memory in treated mice were assessed by a probe test at day 6 (Fig. 6j). Both hINS and AAC2 treated groups exhibited similar responses as the control group (both P=0.1). Overall cognitive performance was only moderately improved by either AAC2 or hINS treatments compared to control group of $Ins2^{Akita}$ mice after short (7 weeks) treatment period.

4. Discussion

Our findings revealed that a specific amino acid compound, AAC2, effectively improved glucose uptake in insulin-insensitive or insulinresistant tissues in T1D and T2D models of diabetes. This compound induced a signaling cascade that differed from the canonic signaling mediated by insulin or leptin. We synthesized a series of AAC compounds by modifying natural amino acids with a range of side-chains, including a coumarin-based antioxidant side chain in the prototype AAC2. Our design consideration was based on the anticipated interactions between amino acid backbone of AAC molecules with receptors regulating glucose metabolism, which could be further enhanced by hydrophobic interactions with the side chain. Our structure-function experiments with several AAC molecules, revealed that both the lysine backbone and a coumarin derivative side chain moiety were necessary and sufficient for the glycemic efficacy of AAC2 in cells from different human and mouse tissues and the absence of toxicity. AAC2 mediated glucose uptake in Lepob model of T2D as well as in Ins2Akita model of T1D. Unexpectedly, AAC2 did not exert a direct antioxidant effect leading to the decrease of ROS. In the future, other coumarin site moieties could be selected to improve the antioxidant action. Antioxidant effects were exhibited by another structure, AAC6, lacking

the coumarin derivative moiety; however, this property was not associated with improved glucose uptake. The prototype AAC2 met our primary criteria for a candidate therapeutic molecule by improving glucose uptake in human cells and animal models of diabetes.

The interaction of AAC2 with LepR was required to mediate glucose uptake. This mechanism was supported by a loss of AAC2 function in cells genetically or functionally deficient in LepR. Moreover, Lepr^{db} mice did not increase glucose uptake in response to AAC2 stimulation and hyperglycemia was more pronounced in ACC2-treated mice than in the control Lepr^{db} mice. AAC2 binding to the recombinant LepR was demonstrated in microbalance experiments, which also revealed different affinities and kinetics of AAC2/LepR interactions compared to the binding of LepR to its established leptin ligand. These different binding characteristics are likely responsible for differences in the downstream signaling cascade induced by AAC2 vs. leptin binding to LepR. The striking difference between AAC2 and leptin signaling was the early onset and prolonged phosphorylation of PKCc/ERK kinases in preadipocytes, which was required for glucose uptake and blocked by PKCc inhibitors. Both leptin and AAC2 utilized the GLUT1 transporter in the insulin-insensitive hBEC. This finding is important because the blood-brain barrier consists of hBEC, which governs glucose influx to the brain and is associated with neurological complications in humans with GLUT1 Deficiency Syndrome [33]. Although the mechanism of AAC2 action was atypical compared to leptin, AAC2 fully substituted for the glycemic action of leptin and effectively improved glucose metabolism in leptin deficient Lepob mice. Other leptin-mediated effects, such as food intake and weight loss were either not replicated by AAC2 or were less pronounced. Based on these data, we conclude that AAC2 is not a mimetic of leptin, but instead, AAC2 acts as a specific agonist for LepR that induces assembly of an alternative signaling pathway for GLUT1-dependent glucose uptake in a cytokine-like manner.

AAC2 appears to be independent of the canonic insulin-induced AKT/GLUT4 pathway and effectively improved glucose metabolism in Ins2Akita model of phenotypes associated with T1D. The different underlying mechanisms of AAC2 and insulin influence physiologic responses in Ins2^{Akita} mice. Insulin induced lipogenic tissue remodeling and increased adiposity in *Ins2*^{Akita} mice. LepR activation is associated with catabolic processes [17]. In agreement, AAC2 treatment did not affect adiposity in the treated Ins2Akita mice. Instead, AAC2 treatment increased brain mass that was associated with the improved functional responses seen as improved anxiety-like behavior. Previous studies demonstrated an association of the increase in rearing behavior with the reduced glucose uptake in the brain [72]. AAC2-mediated glucose uptake by blood-brain barrier endothelial cells seen in our experiments could be at least one mechanism supporting improved responses in neural tissues. However, more studies need to dissect the causative relationship between AAC2 mediated-glucose uptake, PKC5 activation, and neural function. Increased phosphorylation of PKC ς in the brain has been associated with the alleviation of anxiety type of behavior [73]. The effect of AAC2 on cognitive performance was moderate due to the short duration of the treatment period and a relatively early phase of type 1 diabetes in *Ins2*^{Akita} mice. The utilization of alternative pathways by AAC2 could provide a viable strategy to improve glucose uptake regulation in neural and other tissues facing degenerative changes under current treatment regimens. Combinatorial activation of glycemic pathways with insulin, leptin, and AAC2 could especially

improve brain energetics, given a variety of glucose transporters in neural tissue.

Historically, diabetic remedies were based on plant extracts containing anti-inflammatory and anti-inflammatory compounds reducing hyperglycemia [1,47,48,74]. Extracts containing coumarins were used in Ayurvedic medicine to manage symptoms of diabetes [47]. However, a significant improvement in treatment of diabetes began with discovery of insulin [14] and other protein hormones and cytokines [14,75] as well as natural peptides [6]. The majority of 'natural' therapeutic proteins are used in modified forms with improved stability and efficacy in the regulation of glucose metabolism and decreased immunogenicity [14]. The major mechanisms for these therapeutics include mobilization of GLUT4 via AKT, PI3K, and AMPK pathways that allow the control of peripheral glucose metabolism as monitored by hemoglobin A1c (HbA1c) [13,14]. New methods raising insulin levels in the circulation have also been developed, that employ innovative strategies to modify glucagon-like peptide 1 (GLP1) with coumarins [76]. Delivery vehicles have been developed to deliver insulin to the brain [77]. In spite of success in treatment of systemic hyperglycemia with this broad range of therapeutics, the insulinocentric approach to treat nervous tissue is not sufficient to overt neurological and cognitive complications [14].

Synthetic materials continue to be explored as insulin carriers or as protective scaffolds to control insulin release [38]. Nonetheless, a recent study proposed that synthetic implanted porous poly(lactide-coglycolide) scaffolds [78] could possess an inherent property to induce glucose uptake primarily via promoted local secretion of insulin-like growth factor 4 (IGF4), AKT phosphorylation and expression of GLUT1, which increase the local uptake of glucose in adipose tissue in mice. In our AAC design, we took advantage of all these approaches and addressed glucose uptake in the most challenging tissues resistant to natural insulin as well as to insulin-based therapeutics, in insulin-resistant Lepob mice, and insulin deficient Ins2^{Akita} mice. In the first prototype molecule AAC2, both amino acids and coumarin structural components were required for the cytokine-like properties that activated insulin insensitive pathways for glucose uptake in cells of peripheral and nervous tissues. Elucidation of the specific binding sites of LepR for AAC2 was beyond the scope of this proof-of-concept study. In this study, the anti-LepR antibodies abolished both AAC2-dependent and inactivated immunoglobulin-induced glucose uptake in vitro suggesting that AAC2 could act via the immunoglobulin domain of LepR (IGD). IGD activation appears to support only metabolic effects of LepR and is uncoupled from its inflammatory responses, which make it a suitable therapeutic target for diabetes [79]. Focused studies are needed to delineate the AAC2 mechanism for activation of PKCc/ERK/ GLUT1 axes without scavenging of ROS. The rational design of the AAC class of molecules can potentially be used to further improve the properties of AAC2 either by additional modification of the backbone, the site moiety or both. The least explored remained also the nanostructural properties of AAC2, induced by self-assembly that occurs at higher AAC concentrations and may serve as a nanoscaffold for insulin. This supramolecular complex of the AAC2 nanofibers with insulin could have additive or even synergistic therapeutic outcomes. Regardless of these speculations, the mechanism of AAC2 action utilizes catabolic pathways that are potentially compatible with anabolic insulin-centric therapies for balanced glucose delivery to the peripheral tissue and the brain.

5. Conclusion

The clinical features of different forms of diabetes are overlapping [80] and increasingly include neurological degeneration and dementia [81–83]. Insulin resistance and impaired glucose uptake in the brain precedes the onset of dementia years before amyloid pathologies [84–86] emerge. The AAC class of molecules could provide a new strategy for improving glucose delivery to nervous and other tissues

resistant to other therapeutic mediators of glucose uptake for personalized treatment of diabetes and its complications.

Author contributions

A.L. and O.Z. conceived the idea, designed biological experiments, analyzed data, and wrote and edited the manuscript. A.L. performed in vitro and *in vivo* studies. Y.S. and J.R.P. conceived the idea and designed the AACs. T.L. manufactured the AACs, performed transmission electron microscopy (TEM), and participated in harvest of mice samples. N-J S. performed WST-1 assay, ROS-reagents test, and Western blot experiments. M.L.M. characterized nanofiber assembly. J.W., J.H.L, D.K., and A.B. participated in animal studies and harvest of mice samples. J.F., A.C.D, R.J.N., and Z.W. performed, analyzed, and supervised cognitive function tests. L.A.B. and K.I.S. performed CLAMS. B.N. and S.N. collected human fat tissues. J.O-A. and R.J.F. performed and supervised the QCM-D assay. L.G-D and J.J.B. developed analytical method. All authors contributed to the discussion, editing, and reviewing the manuscript.

Data availability

The datasets generated during and/or analyzed during the current study are available from the corresponding author on reasonable request.

Declaration of competing interest

The authors declare no competing financial interests.

Acknowledgements

We are grateful to David Szarvas (OSU), Shiyam Vashi (OSU), and Ariana Parquette (OSU) for their excellent help with the animal experiments. We also would like to thank Andrew Suzo (OSU) and Kayla Diaz (OSU) for their help for coordination of work with human samples. We would like to thank Mariana Ponte for her help with animal experiments. Dr. Ortega-Anaya and Dr. Jiménez-Flores acknowledge aid given by the JT Parker Endowment to OSU. The project was supported by the Dr. Ralph and Marian Falk Medical Research Trust Catalyst Awards Program (J.R.P., O.Z.), an Accelerator Award from the Technology and Commercialization Office at OSU (J.R.P., O.Z., A.L.), and the National Science Foundation (CHE-1412295, J.R.P.). We also acknowledge the Center of Applied Plant Sciences at OSU and the National Center for Research Resources UL1RR025755, UL1TR001070, and NCI P30CA16058 (OSUCCC), and the NIH Roadmap for Medical Research. K.I.S was supported by R01-HL138738. The content is solely the responsibility of the authors and does not necessarily represent the official views of the National Center for Research Resources or the National Institutes of Health.

Appendix A. Supplementary data

Supplementary data to this article can be found online at https://doi.org/10.1016/j.biomaterials.2020.119839.

References

- [1] K. Noipha, T. Thongthoom, U. Songsiang, C. Boonyarat, C. Yenjai, Carbazoles and coumarins from Clausena harmandiana stimulate glucose uptake in L6 myotubes, Diabetes Res. Clin. Pract. 90 (3) (2010) e67–71.
- [2] A. Priyanka, G.L. Shyni, N. Anupama, P.S. Raj, S.S. Anusree, K.G. Raghu, Development of insulin resistance through sprouting of inflammatory markers during hypoxia in 3T3-L1 adipocytes and amelioration with curcumin, Eur. J. Pharmacol. 812 (2017) 73–81.
- [3] A. Bolsoni-Lopes, W.T. Festuccia, P. Chimin, T.S. Farias, F.L. Torres-Leal, M.M. Cruz, P.B. Andrade, S.M. Hirabara, F.B. Lima, M.I. Alonso-Vale, Palmitoleic acid (n-7) increases white adipocytes GLUT4 content and glucose uptake in

- association with AMPK activation, Lipids Health Dis. 13 (2014) 199.
- [4] S. Nishitani, K. Takehana, S. Fujitani, I. Sonaka, Branched-chain amino acids improve glucose metabolism in rats with liver cirrhosis, Am. J. Physiol. Gastrointest. Liver Physiol. 288 (6) (2005) G1292–G1300.
- [5] M.J. Cripps, K. Hanna, C. Lavilla Jr., S.R. Sayers, P.W. Caton, C. Sims, L. De Girolamo, C. Sale, M.D. Turner, Carnosine scavenging of glucolipotoxic free radicals enhances insulin secretion and glucose uptake, Sci. Rep. 7 (1) (2017) 13313.
- [6] T. Ayabe, T. Mizushige, W. Ota, F. Kawabata, K. Hayamizu, L. Han, T. Tsuji, R. Kanamoto, K. Ohinata, A novel Alaska pollack-derived peptide, which increases glucose uptake in skeletal muscle cells, lowers the blood glucose level in diabetic mice, Food Funct 6 (8) (2015) 2749–2757.
- [7] S.I. Ikeda, Y. Tamura, S. Kakehi, H. Sanada, R. Kawamori, H. Watada, Exercise-induced increase in IL-6 level enhances GLUT4 expression and insulin sensitivity in mouse skeletal muscle, Biochem. Biophys. Res. Commun. 473 (4) (2016) 947–952.
- [8] K. Li, L. Li, M. Yang, H. Liu, G. Boden, G. Yang, The effects of fibroblast growth factor-21 knockdown and over-expression on its signaling pathway and glucoselipid metabolism in vitro, Mol. Cell. Endocrinol. 348 (1) (2012) 21–26.
- [9] T. Lan, D.A. Morgan, K. Rahmouni, J. Sonoda, X. Fu, S.C. Burgess, W.L. Holland, S.A. Kliewer, D.J. Mangelsdorf, FGF19, FGF21, and an FGFR1/beta-klotho-activating antibody act on the nervous system to regulate body weight and glycemia, Cell Metabol. 26 (5) (2017) 709–718 e3.
- [10] P. Bostrom, J. Wi, M.P. Jedrychowski, A. Korde, L. Ye, J.C. Lo, K.A. Rasbach, E.A. Bostrom, J.H. Choi, J.Z. Long, S. Kajimura, M.C. Zingaretti, B.F. Vind, H. Tu, S. Cinti, K. Hojlund, S.P. Gygi, B.M. Spiegelman, A PGC1-alpha-dependent myokine that drives brown-fat-like development of white fat and thermogenesis, Nature 481 (7382) (2012) 463–468.
- [11] L. Cao, X. Liu, E.J. Lin, C. Wang, E.Y. Choi, V. Riban, B. Lin, M.J. During, Environmental and genetic activation of a brain-adipocyte BDNF/leptin axis causes cancer remission and inhibition, Cell 142 (1) (2010) 52–64.
- [12] A. Ali Khan, J. Hansson, P. Weber, S. Foehr, J. Krijgsveld, S. Herzig, M. Scheideler, Comparative secretome analyses of primary murine white and Brown adipocytes reveal novel adipokines, Mol. Cell. Proteomics 17 (12) (2018) 2358–2370.
- [13] C.R. Kahn, The Gordon Wilson Lecture. Lessons about the control of glucose homeostasis and the pathogenesis of diabetes from knockout mice, Trans. Am. Clin. Climatol. Assoc. 114 (2003) 125–148.
- [14] A.N. Zaykov, J.P. Mayer, R.D. DiMarchi, Pursuit of a perfect insulin, Nature reviews, Drug discovery 15 (6) (2016) 425–439.
- [15] D.A. Dionne, S. Skovso, N.M. Templeman, S.M. Clee, J.D. Johnson, Caloric restriction paradoxically increases adiposity in mice with genetically reduced insulin, Endocrinology 157 (7) (2016) 2724–2734.
- [16] L. Berti, S. Gammeltoft, Leptin stimulates glucose uptake in C2C12 muscle cells by activation of ERK2, Mol. Cell. Endocrinol. 157 (1–2) (1999) 121–130.
- [17] Y. Ravussin, R.L. Leibel, A.W. Ferrante Jr., A missing link in body weight homeostasis: the catabolic signal of the overfed state, Cell Metabol. 20 (4) (2014) 565–572.
- [18] B.B. Kahn, Adipose tissue, inter-organ communication, and the path to type 2 diabetes: the 2016 banting medal for scientific achievement lecture, Diabetes 68 (1) (2019) 3–14
- [19] J. Wauman, L. Zabeau, J. Tavernier, The leptin receptor complex: heavier than expected? Front. Endocrinol. 8 (2017) 30.
- [20] S.T. Azar, P.A. Zalloua, M.S. Zantout, C.H. Shahine, I. Salti, Leptin levels in patients with type 1 diabetes receiving intensive insulin therapy compared with those in patients receiving conventional insulin therapy, J. Endocrinol. Invest. 25 (8) (2002) 724–726.
- [21] R.J. Perry, X.M. Zhang, D. Zhang, N. Kumashiro, J.P. Camporez, G.W. Cline, D.L. Rothman, G.I. Shulman, Leptin reverses diabetes by suppression of the hypothalamic-pituitary-adrenal axis, Nat. Med. 20 (7) (2014) 759–763.
- [22] X. Yu, B.H. Park, M.Y. Wang, Z.V. Wang, R.H. Unger, Making insulin-deficient type 1 diabetic rodents thrive without insulin, Proc. Natl. Acad. Sci. U. S. A. 105 (37) (2008) 14070–14075.
- [23] I. Shimomura, R.E. Hammer, S. Ikemoto, M.S. Brown, J.L. Goldstein, Leptin reverses insulin resistance and diabetes mellitus in mice with congenital lipodystrophy, Nature 401 (6748) (1999) 73–76.
- [24] K. Ebihara, T. Kusakabe, M. Hirata, H. Masuzaki, F. Miyanaga, N. Kobayashi, T. Tanaka, H. Chusho, T. Miyazawa, T. Hayashi, K. Hosoda, Y. Ogawa, A.M. DePaoli, M. Fukushima, K. Nakao, Efficacy and safety of leptin-replacement therapy and possible mechanisms of leptin actions in patients with generalized lipodystrophy, J. Clin. Endocrinol. Metabol. 92 (2) (2007) 532–541.
- [25] G.S. Watson, S. Craft, Modulation of memory by insulin and glucose: neuropsychological observations in Alzheimer's disease, Eur. J. Pharmacol. 490 (1–3) (2004) 97–113.
- [26] S. Camandola, M.P. Mattson, Brain metabolism in health, aging, and neurodegeneration, EMBO J. 36 (11) (2017) 1474–1492.
- [27] D.A. McClain, M. Hazel, G. Parker, R.C. Cooksey, Adipocytes with increased hexosamine flux exhibit insulin resistance, increased glucose uptake, and increased synthesis and storage of lipid, Am. J. Physiol. Endocrinol. Metab. 288 (5) (2005) E973–E979.
- [28] S. Morgello, R.R. Uson, E.J. Schwartz, R.S. Haber, The human blood-brain barrier glucose transporter (GLUT1) is a glucose transporter of gray matter astrocytes, Glia 14 (1) (1995) 43–54.
- [29] C.W. Heilig, T. Saunders, F.C. Brosius 3rd, K. Moley, K. Heilig, R. Baggs, L. Guo, D. Conner, Glucose transporter-1-deficient mice exhibit impaired development and deformities that are similar to diabetic embryopathy, Proc. Natl. Acad. Sci. U. S. A. 100 (26) (2003) 15613–15618.
- [30] D.C. De Vivo, R.R. Trifiletti, R.I. Jacobson, G.M. Ronen, R.A. Behmand, S.I. Harik, Defective glucose transport across the blood-brain barrier as a cause of persistent

- hypoglycorrhachia, seizures, and developmental delay, N. Engl. J. Med. 325 (10) (1991) 703–709.
- [31] T.J. Han, H.Z. Xu, J.S. Li, L.Y. Geng, X.Y. Li, X.X. Zhou, X. Wang, Leptin and its receptor in glucose metabolism of T-cell lymphoma, Oncol Lett 16 (5) (2018) 5838–5846.
- [32] A.V. Mathew, M. Jaiswal, L. Ang, G. Michailidis, S. Pennathur, R. Pop-Busui, Impaired Amino Acid and TCA Metabolism and Cardiovascular Autonomic Neuropathy Progression in Type 1 Diabetes, Diabetes (2019).
- [33] E.E. Lee, J. Ma, A. Sacharidou, W. Mi, V.K. Salato, N. Nguyen, Y. Jiang, J.M. Pascual, P.E. North, P.W. Shaul, M. Mettlen, R.C. Wang, A protein kinase C phosphorylation motif in GLUT1 affects glucose transport and is mutated in GLUT1 deficiency Syndrome, Mol. Cell 58 (5) (2015) 845–853.
- [34] S. Schmidt, V. Gawlik, S.M. Holter, R. Augustin, A. Scheepers, M. Behrens, W. Wurst, V. Gailus-Durner, H. Fuchs, M. Hrabe de Angelis, R. Kluge, H.G. Joost, A. Schurmann, Deletion of glucose transporter GLUT8 in mice increases locomotor activity, Behav. Genet. 38 (4) (2008) 396–406.
- [35] M. Schubert, D. Gautam, D. Surjo, K. Ueki, S. Baudler, D. Schubert, T. Kondo, J. Alber, N. Galldiks, E. Kustermann, S. Arndt, A.H. Jacobs, W. Krone, C.R. Kahn, J.C. Bruning, Role for neuronal insulin resistance in neurodegenerative diseases, Proc. Natl. Acad. Sci. U. S. A. 101 (9) (2004) 3100–3105.
- [36] Y. Benomar, N. Naour, A. Aubourg, V. Bailleux, A. Gertler, J. Djiane, M. Guerre-Millo, M. Taouis, Insulin and leptin induce Glut4 plasma membrane translocation and glucose uptake in a human neuronal cell line by a phosphatidylinositol 3-kinase-dependent mechanism, Endocrinology 147 (5) (2006) 2550–2556.
- [37] G.J. Boersma, E. Johansson, M.J. Pereira, K. Heurling, S. Skrtic, J. Lau, P. Katsogiannos, G. Panagiotou, M. Lubberink, J. Kullberg, H. Ahlstrom, J.W. Eriksson, Altered glucose uptake in muscle, visceral adipose tissue, and brain predict whole-body insulin resistance and may contribute to the development of type 2 diabetes: a combined PET/MR study, Horm. Metab. Res. 50 (8) (2018) 627–639.
- [38] R.A. Tromans, T.S. Carter, L. Chabanne, M.P. Crump, H. Li, J.V. Matlock, M.G. Orchard, A.P. Davis, A biomimetic receptor for glucose, Nat. Chem. 11 (1) (2019) 52–56.
- [39] S.E. Arnold, Z. Arvanitakis, S.L. Macauley-Rambach, A.M. Koenig, H.Y. Wang, R.S. Ahima, S. Craft, S. Gandy, C. Buettner, L.E. Stoeckel, D.M. Holtzman, D.M. Nathan, Brain insulin resistance in type 2 diabetes and Alzheimer disease: concepts and conundrums, Nat. Rev. Neurol. (2018).
- [40] C.T. Kodl, E.R. Seaquist, Cognitive dysfunction and diabetes mellitus, Endocr. Rev. 29 (4) (2008) 494–511.
- [41] G.J. Biessels, F. Despa, Cognitive decline and dementia in diabetes mellitus: mechanisms and clinical implications, Nat. Rev. Endocrinol. 14 (10) (2018) 591–604.
- [42] E.A. Northam, P.J. Anderson, G.A. Werther, G.L. Warne, R.G. Adler, D. Andrewes, Neuropsychological complications of IDDM in children 2 years after disease onset, Diabetes Care 21 (3) (1998) 379–384.
- [43] L. Mosconi, V. Berti, L. Glodzik, A. Pupi, S. De Santi, M.J. de Leon, Pre-clinical detection of Alzheimer's disease using FDG-PET, with or without amyloid imaging, J Alzheimers Dis 20 (3) (2010) 843–854.
- [44] S. Yibchok-anun, S. Adisakwattana, C.Y. Yao, P. Sangvanich, S. Roengsumran, W.H. Hsu, Slow acting protein extract from fruit pulp of Momordica charantia with insulin secretagogue and insulinomimetic activities, Biol. Pharm. Bull. 29 (6) (2006) 1126–1131.
- [45] D. Kalogeropoulou, L. LaFave, K. Schweim, M.C. Gannon, F.Q. Nuttall, Lysine ingestion markedly attenuates the glucose response to ingested glucose without a change in insulin response, Am. J. Clin. Nutr. 90 (2) (2009) 314–320.
- [46] R.J. Marles, N.R. Farnsworth, Antidiabetic plants and their active constituents, Phytomedicine 2 (2) (1995) 137–189.
- [47] H. Li, Y. Yao, L. Li, Coumarins as potential antidiabetic agents, J. Pharm. Pharmacol. 69 (10) (2017) 1253–1264.
- [48] K.C. Fylaktakidou, D.J. Hadjipavlou-Litina, K.E. Litinas, D.N. Nicolaides, Natural and synthetic coumarin derivatives with anti-inflammatory/antioxidant activities, Curr. Pharmaceut. Des. 10 (30) (2004) 3813–3833.
- [49] A. Kaur, M.A. Haghighatbin, C.F. Hogan, E.J. New, A FRET-based ratiometric redox probe for detecting oxidative stress by confocal microscopy, FLIM and flow cytometry, Chem. Comm. 51 (52) (2015) 10510–10513.
- [50] Y. Sun, J.A. Kaplan, A. Shieh, H.L. Sun, C.M. Croce, M.W. Grinstaff, J.R. Parquette, Self-assembly of a 5-fluorouracil-dipeptide hydrogel, Chem. Comm. 52 (30) (2016) 5254–5257.
- [51] R. Yasmeen, B. Reichert, J. Deiuliis, F. Yang, A. Lynch, J. Meyers, M. Sharlach, S. Shin, K.S. Volz, K.B. Green, K. Lee, H. Alder, G. Duester, R. Zechner, S. Rajagopalan, O. Ziouzenkova, Autocrine function of aldehyde dehydrogenase 1 as a determinant of diet- and sex-specific differences in visceral adiposity, Diabetes 62 (1) (2013) 124–136.
- [52] M.D. Ward, D.A. Buttry, In situ interfacial mass detection with piezoelectric transducers, Science 249 (4972) (1990) 1000–1007.
- [53] S.F. Hedegaard, M. Cardenas, R. Barker, L. Jorgensen, M. van de Weert, Lipidation effect on surface adsorption and associated fibrillation of the model protein insulin, Langmuir: ACS J. Surface. Colloids 32 (28) (2016) 7241–7249.
- [54] M.V. Voinova, M. Rodahl, M. Jonson, B. Kasemo, Viscoelastic acoustic response of layered polymer films at fluid-solid interfaces: continuum mechanics approach, Phys. Scripta 59 (5) (1999) 391–396.
- [55] I. Reviakine, D. Johannsmann, R.P. Richter, Hearing what you cannot see and visualizing what you hear: interpreting quartz crystal microbalance data from solvated interfaces, Anal. Chem. 83 (23) (2011) 8838–8848.
- [56] A.I. Hernandez, N. Blace, J.F. Crary, P.A. Serrano, M. Leitges, J.M. Libien, G. Weinstein, A. Tcherapanov, T.C. Sacktor, Protein kinase M zeta synthesis from a brain mRNA encoding an independent protein kinase C zeta catalytic domain.

- Implications for the molecular mechanism of memory, J. Biol. Chem. 278 (41) (2003) 40305–40316.
- [57] J.C. Walton, Z. Chen, Z.M. Weil, L.M. Pyter, J.B. Travers, R.J. Nelson, Photoperiod-mediated impairment of long-term potention and learning and memory in male white-footed mice, Neuroscience 175 (2011) 127–132.
- [58] H. Shao, T. Nguyen, N.C. Romano, D.A. Modarelli, J.R. Parquette, Self-assembly of 1-D n-type nanostructures based on naphthalene diimide-appended dipeptides, J. Am. Chem. Soc. 131 (45) (2009) 16374–16376.
- [59] R.J. Weaver, J.P. Valentin, Today's challenges to de-risk and predict drug safety in human "mind-the-gap", Toxicol. Sci. 167 (2) (2019) 307–321.
- [60] T. Caputo, F. Gilardi, B. Desvergne, From chronic overnutrition to metaflammation and insulin resistance: adipose tissue and liver contributions, FEBS Lett. 591 (19) (2017) 3061–3088.
- [61] D. Virgintino, D. Robertson, P. Monaghan, M. Errede, M. Bertossi, G. Ambrosi, L. Roncali, Glucose transporter GLUT1 in human brain microvessels revealed by ultrastructural immunocytochemistry, J. Submicr. Cytol. Pathol. 29 (3) (1997) 365–370
- [62] M.A. Khokher, P. Dandona, Stimulatory effect of immunoglobulins and Fc fragments on glucose oxidation and glucose transport by adipocytes, Br. J. Exp. Pathol. 66 (2) (1985) 129–135.
- [63] C.M. Taniguchi, B. Emanuelli, C.R. Kahn, Critical nodes in signalling pathways: insights into insulin action, Nature reviews, Mol. Cell Biol. 7 (2) (2006) 85–96.
- [64] T. Saito, S. Okada, Y. Shimoda, Y. Tagaya, A. Osaki, E. Yamada, R. Shibusawa, Y. Nakajima, A. Ozawa, T. Satoh, M. Mori, M. Yamada, APPL1 promotes glucose uptake in response to mechanical stretch via the PKCzeta-non-muscle myosin IIa pathway in C2C12 myotubes, Cell. Signal. 28 (11) (2016) 1694–1702.
- [65] J.M. Friedman, C.S. Mantzoros, 20 years of leptin: from the discovery of the leptin gene to leptin in our therapeutic armamentarium, Metabolism 64 (1) (2015) 1–4.
- [66] R. Muzumdar, X. Ma, X. Yang, G. Atzmon, J. Bernstein, G. Karkanias, N. Barzilai, Physiologic effect of leptin on insulin secretion is mediated mainly through central mechanisms, FASEB J 17 (9) (2003) 1130–1132.
- [67] T.L. Van Belle, P. Taylor, M.G. von Herrath, Mouse models for type 1 diabetes, drug discovery today, Dis. Models 6 (2) (2009) 41–45.
- [68] J. Wang, T. Takeuchi, S. Tanaka, S.K. Kubo, T. Kayo, D. Lu, K. Takata, A. Koizumi, T. Izumi, A mutation in the insulin 2 gene induces diabetes with severe pancreatic beta-cell dysfunction in the Mody mouse, J. Clin. Invest. 103 (1) (1999) 27–37.
- [69] K.A. Sullivan, S.I. Lentz, J.L. Roberts Jr., E.L. Feldman, Criteria for creating and assessing mouse models of diabetic neuropathy, Curr. Drug Targets 9 (1) (2008) 3–13.
- [70] J.A. Brown, A. Wright, R. Bugescu, L. Christensen, D.P. Olson, G.M. Leinninger, Distinct subsets of lateral hypothalamic neurotensin neurons are activated by leptin or dehydration, Sci. Rep. 9 (1) (2019) 1873.
- [71] H. Caliskan, F. Akat, Y. Tatar, N. Zaloglu, A.D. Dursun, H. Ficicilar, M. Bastug, Effects of exercise training on anxiety in diabetic rats, Behav. Brain Res. (2019) 112084.
- [72] E.L. Aguirre-Benitez, M.G. Porras, L. Parra, J. Gonzalez-Rios, D.F. Garduno-Torres, D. Albores-Garcia, A. Avendano, M.A. Avila-Rodriguez, A.I. Melo, I. Jimenez-Estrada, M.E. Mendoza-Garrido, C. Toriz, D. Diaz, E. Ibarra-Coronado, K. Mendoza-Angeles, J. Hernandez-Falcon, Disruption of behavior and brain metabolism in artificially reared rats. Dev. Neurobiol. 77 (12) (2017) 1413–1429.

[73] J. Du, J. Fang, C. Wen, X. Shao, Y. Liang, J. Fang, The effect of electroacupuncture on PKMzeta in the ACC in regulating anxiety-like behaviors in rats experiencing chronic inflammatory pain, Neural Plast. 2017 (2017) 3728752.

- [74] H. Cao, Y. Ji, W. Li, Y. Liu, R. Fu, M. Xiang, Protective effects of the total coumarin fraction of urtica dentata on experimental diabetic nephropathy in vitro and in vivo, Planta Med. 81 (15) (2015) 1353–1360.
- [75] W. Aoi, N. Hirano, D.G. Lassiter, M. Bjornholm, A.V. Chibalin, K. Sakuma, Y. Tanimura, K. Mizushima, T. Takagi, Y. Naito, J.R. Zierath, A. Krook, Secreted protein acidic and rich in cysteine (SPARC) improves glucose tolerance via AMPactivated protein kinase activation, FASEB J (2019) fj201900453R.
- [76] J. Han, L. Sun, X. Huang, Z. Li, C. Zhang, H. Qian, W. Huang, Novel coumarin modified GLP-1 derivatives with enhanced plasma stability and prolonged in vivo glucose-lowering ability, Br. J. Pharmacol. 171 (23) (2014) 5252–5264.
- [77] J. Wingrove, M. Swedrowska, R. Scherliess, M. Parry, M. Ramjeeawon, D. Taylor, G. Gauthier, L. Brown, S. Amiel, F. Zelaya, B. Forbes, Characterisation of nasal devices for delivery of insulin to the brain and evaluation in humans using functional magnetic resonance imaging, J. Contr. Release 302 (2019) 140–147.
- [78] M.A. Hendley, K.P. Murphy, C. Isely, H.L. Struckman, P. Annamalai, R.M. Gower, The host response to poly(lactide-co-glycolide) scaffolds protects mice from diet induced obesity and glucose intolerance, Biomaterials 217 (2019) 119281.
- [79] L. Zabeau, C.J. Jensen, S. Seeuws, K. Venken, A. Verhee, D. Catteeuw, G. van Loo, H. Chen, K. Walder, J. Hollis, S. Foote, M.J. Morris, J. Van der Heyden, F. Peelman, B.J. Oldfield, J.P. Rubio, D. Elewaut, J. Tavernier, Leptin's metabolic and immune functions can be uncoupled at the ligand/receptor interaction level, Cell. Mol. Life Sci.: CMLS 72 (3) (2015) 629–644.
- [80] E. Castelblanco, M. Hernandez, A. Castelblanco, M. Gratacos, A. Esquerda, A. Mollo, A. Ramirez-Morros, J. Real, J. Franch-Nadal, J.M. Fernandez-Real, D. Mauricio, Low-grade Inflammatory Marker Profile May Help to Differentiate Patients with LADA, Classic Adult-Onset Type 1 and Type 2 Diabetes, Diabetes care, 2018.
- [81] K. Smolina, C.J. Wotton, M.J. Goldacre, Risk of dementia in patients hospitalised with type 1 and type 2 diabetes in England, 1998-2011: a retrospective national record linkage cohort study, Diabetologia 58 (5) (2015) 942-950.
- [82] A.L. Emanuel, M.D. Nieuwenhoff, E.S. Klaassen, A. Verma, M.H. Kramer, R. Strijers, A.F. Vrancken, E. Eringa, G.J. Groeneveld, E.H. Serne, Relationships between type 2 diabetes, neuropathy, and microvascular dysfunction: evidence from patients with cryptogenic axonal polyneuropathy, Diabetes Care 40 (4) (2017) 583–590.
- [83] L.G. Rodill, L.G. Exalto, P. Gilsanz, G.J. Biessels, C.P. Quesenberry Jr., R.A. Whitmer, Diabetic Retinopathy and Dementia in Type 1 Diabetes, Alzheimer Disease and Associated Disorders, (2017).
- [84] L. Iaccarino, K. Chiotis, P. Alongi, O. Almkvist, A. Wall, C. Cerami, V. Bettinardi, L. Gianolli, A. Nordberg, D. Perani, A cross-validation of FDG- and amyloid-PET biomarkers in mild cognitive impairment for the risk prediction to dementia due to alzheimer's disease in a clinical setting, J Alzheimers Dis 59 (2) (2017) 603–614.
- [85] A.A. Willette, B.B. Bendlin, E.J. Starks, A.C. Birdsill, S.C. Johnson, B.T. Christian, O.C. Okonkwo, A. La Rue, B.P. Hermann, R.L. Koscik, E.M. Jonaitis, M.A. Sager, S. Asthana, Association of insulin resistance with cerebral glucose uptake in late middle-aged adults at risk for alzheimer disease, JAMA Neurol. 72 (9) (2015) 1013–1020.
- [86] D.A. Butterfield, B. Halliwell, Oxidative stress, dysfunctional glucose metabolism and Alzheimer disease, Nat. Rev. Neurosci. 20 (3) (2019) 148–160.